Electron transport of inhomogeneous Schottky barriers: A numerical study

J. P. Sullivan,[a] R. T. Tung, and M. R. Pinto
AT&T Bell Laboratories, Murray Hill, New Jersey 07974

W. R. Graham
Department of Materials Science & Engineering, University of Pennsylvania, Philadelphia, Pennsylvania 19104

(Received 8 July 1991; accepted for publication 18 September 1991)

Numerical simulations are presented of the potential distribution and current transport associated with metal-semiconductor (MS) contacts in which the Schottky barrier height (SBH) varies spatially. It is shown that the current across the MS contact may be greatly influenced by the existence of SBH inhomogeneity. Numerical simulations indicate that regions of low SBH are often pinched-off when the size of these regions is less than the average depletion width. Saddle points in the potential contours in close proximity to the low-SBH regions, which are shown to vary with the dimension and magnitude of the inhomogeneity as well as with bias, essentially determine the electron transport across the low-SBH regions. It is these dependences of the saddle point which give rise to various abnormal behaviors frequently observed from SBH experiments, such as ideality factors greater than unity, various temperature dependences of the ideality factor, including the T_0 anomaly, and reverse characteristics which are strongly bias-dependent. The results of these numerical simulations are shown to support the predictions of a recently developed analytic theory of SBH inhomogeneity.

I. INTRODUCTION

Much of our understanding of metal-semiconductor (MS) contacts is derived from the electrical characterization of Schottky barrier (SB) contacts. Virtually all theoretical attempts to understand the origin of the Schottky barrier height (SBH), defined as the difference in energy between the metal Fermi level (FL) and the nearest delocalized state of the majority carrier at the MS interface, have implicitly assumed the existence of a uniform electronic structure at the interface. In particular, the suggestion that the SBH is determined by the pinning of the FL by interface states within the semiconductor band gap is well known.[1,2] As a result, theoretical models have focused on the issue of what controls the interface state distribution with respect to the semiconductor. Popular theories attribute these interface states to metal-induced gap states,[3] or to defect states in the semiconductor.[4] In these theories, there is no direct account taken of the possible influence of spatial nonuniformities in the characteristics of the MS interface.

Experimentally, the interpretation of electrical data from real MS contacts has implicitly assumed the uniformity of the SBH at the MS interface. The electrical characterization of real MS contacts, however, is often beset with a number of inconsistencies. For example, the ideality factor, n, of current-voltage (I-V) curves often deviates significantly from unity (the ideal theories of current transport based on thermionic emission or drift-diffusion predict an ideality factor of unity[5]). Other inconsistencies include the T_0 anomaly (a dependence of the ideality factor on temperature of the form $n = 1 + T_0/T$, where T_0 is a temperature-independent constant), the existence of excess current at low bias as observed in I-V plots, the discrepancy between I-V and capacitance-voltage (C-V) determined barrier heights, and soft reverse characteristics (the incomplete saturation of the reverse current). Some empirical explanations exist for most of these anomalies or inconsistencies. For example, current transport based on generation-recombination current predicts an ideality factor of 2,[6] a distribution in interface electronic states or an inversion layer at the MS interface have been proposed as possible explanations of the T_0 anomaly,[7,8] recombination current associated with high fields at the depletion edges has been proposed as a possible source for excess current observed at low bias,[9] and image force lowering can account for some of the observed soft reverse characteristics.[10] However, there has been no theory which is capable of explaining all of these inconsistencies in a coherent manner. We will show, through numerical simulations of inhomogeneous MS contacts, that all of the electrical anomalies mentioned above may be attributed to the presence of SBH inhomogeneity.

At this point, no *a priori* assumption of the underlying cause of the SBH inhomogeneity will be made. It is sufficient to note that the SBH is likely a function of the interface atomic structure,[11–13] and that in virtually all MS contacts there is at least some form of atomic inhomogeneity at the MS interface (e.g., grain boundaries, multiple phases, facets, defects, etc.). The numerical simulations are organized into four main sections. In the next section, we will discuss how the numerical simulations were performed and what assumptions and physical models were used. Then we will present numerical simulations of the potential distribution associated with MS contacts in which there is a spatial variation of the SBH at the MS interface.

[a]Permanent address: Department of Materials Science & Engineering, University of Pennsylvania, Philadelphia, PA 19104.

 0021-8979/91/127403-22$03.00

Following this section, we present numerical simulations of the current transport through a single region of low SBH. It will be shown that the current transport through a low-SBH "patch" is dependent on the patch geometry and dimensions, the substrate doping, the temperature, and the magnitude of the interfacial SBH difference. In the final section of numerical simulations, we present simulations of the total current flowing through MS contacts which contain a variety of distributions of low-SBH patches. From these numerical simulations, it is possible to understand the origin of many of the anomalies discussed above. Throughout the discussion, we compare the numerical simulations with a recently developed analytic theory of SBH inhomogeneity.[14] It is shown that the numerical results are well-described by the analytic theory.

II. METHODS OF THE NUMERICAL SIMULATIONS

The potential and current transport numerical simulations for inhomogeneous MS contacts were performed using PADRE, a general-purpose, multidimensional device simulator.[15,16] PADRE solves the Poisson equation along with the partial differential equations (PDEs) derived from moments of the Boltzmann transport equation for structures with arbitrary two-dimensional/three-dimensional (2D/3D) geometries and material composition, including heterostructures. The PDEs are discretized in space using an element-based, generalized box method including upwinding of the transport equations. PADRE uses simplicial grid elements (triangles in 2D, tetrahedra in 3D) with local, error-based adaption in order to efficiently represent nonplanarities and internal nonlinearities (for the simple device structures of the MS contacts, a fixed grid structure was used; see below). The discretized equations are solved using Newton and sparse linear (direct and iterative) methods which effectively treat the strong coupling between PDEs and achieve near-optimal performance on vector/parallel computers.

Because nonequilibrium energy-related effects such as velocity overshoot are not relevant in the bulk of the MS structures of interest, the convenient drift-diffusion system, consisting of Poisson's equation and continuity equations for each carrier,[5] was selected for use in this study. The effect of acoustic phonon and ionized impurity scattering was incorporated by taking the carrier mobility, μ, at the position $\mathbf{x} = (x,y,z)$ to be a function of the lattice temperature, T, and local impurity concentration at $\mathbf{x}$, $N(\mathbf{x})$,

$$\mu(\mathbf{x}) = \left(\frac{\mu_1 - \mu_2}{1 + (T/300)^{-\gamma}(N(\mathbf{x})/N_1)^{\zeta}} + \mu_2\right) \cdot \left(\frac{T}{300}\right)^{-\alpha}. \tag{1}$$

Most examples below involve diodes on n-type Si, for which the fitting parameters, $\mu_1 = 1390$ cm^2/V s, $\mu_2 = 55.24$ cm^2/V s, $\gamma = 3.8$, $N_1 = 1.072 \times 10^{17}$ cm^{-3}, $\zeta = 0.733$ and $\alpha = 2.3$, reproduce the resistivities observed experimentally.[15] Both Auger and Shockley–Read–Hall (SRH) recombination mechanisms were included, and the minority-carrier lifetime for SRH was also given a dependence on $N(\mathbf{x})$

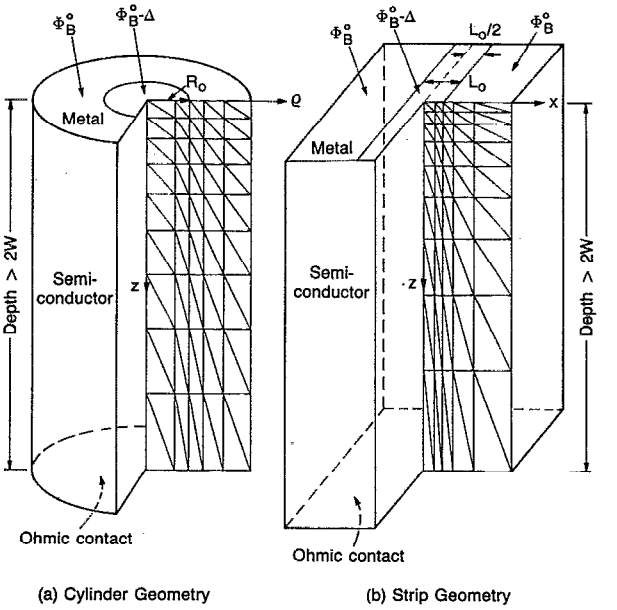

FIG. 1. Geometries of the inhomogeneous MS contacts used in the numerical simulations: (a) cylinder geometry, (b) strip geometry.

$$\tau_{\mathrm{SRH}}(\mathbf{x}) = \frac{\tau_0}{1 + N(\mathbf{x})/N_2}. \tag{2}$$

In all of the n-type Si examples to follow we have used the constants $\tau_0 = 0.5$ μs and $N_2 = 5 \times 10^{16}$ cm^{-3}. For other semiconductors, appropriate values from the database of PADRE were used.[15]

PADRE contains comprehensive models for Schottky contacts including finite surface recombination velocities and barrier lowering as an arbitrary nonlinear function of the normal field. In this study the SBH was always fixed, yielding a Dirichlet boundary condition at the front and back (assumed Ohmic) contacts. Additionally an infinite surface recombination was assumed (i.e., $\phi_n = \phi_p = V_a$, where V_a is the applied bias). Homogeneous Neumann boundary conditions ($\mathbf{E}\cdot\mathbf{n} = 0$, $\mathbf{J}\cdot\mathbf{n} = 0$) were assumed on all noncontact edges of the device. The device depth was always taken to be at least twice the maximum depletion width, and the grid and discretization error were selected such that further refinement had no noticeable effect on the results presented.

Because of symmetry, three dimensional simulations of the potential and transport behavior at inhomogeneous SBs for the geometries we have selected only required the use of properly weighted, two-dimensional meshes. Two primary geometries for the simulation of MS contacts with SBH inhomogeneity were considered (see Fig. 1). For most simulations, a cylindrical geometry for the SBH inhomogeneity was used. In this geometry, a circular region with a SBH of $\Phi_B^0 - \Delta$, and radius $\rho = R_0$, is surrounded by an annulus of higher SBH, Φ_B^0. Distance into the semiconductor is taken to be the positive z direction. An Ohmic contact is situated at a depth greater than twice the semiconductor depletion width. Because of the azimuthal

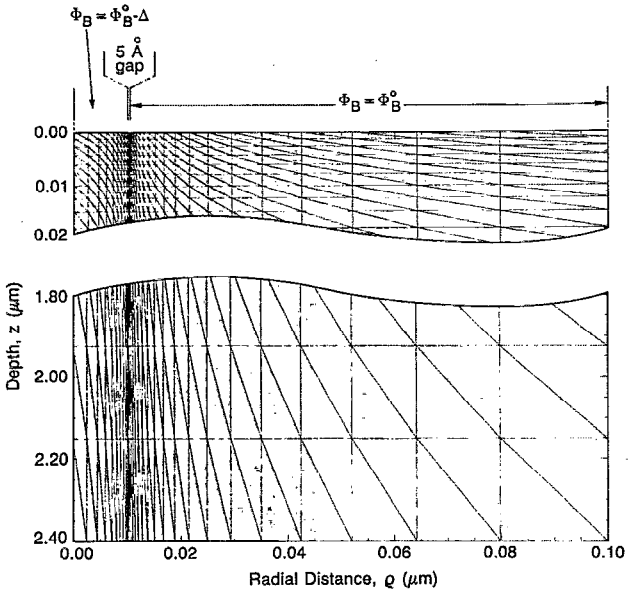

FIG. 2. Typical structure of the mesh used in the simulations of inhomogeneous MS contacts with cylindrical symmetry. Dirichlet boundary conditions are used at the MS interface and backside contact, while Neumann boundary conditions are used at the contact-free mesh boundaries. A total semiconductor thickness in excess of twice the maximum semiconductor depletion width is used. The vertical scale in the bottom portion of the mesh is shown increased by a factor of 10.

symmetry of this geometry, only a 2-D mesh is required to uniquely determine the potentials and currents for the entire structure, thus saving a substantial amount of computation time. The mesh boundaries used in the simulations are defined by a radial line centered at the low-SBH patch ($\rho = 0$, $z = 0$) and by the axial line, defined by $\rho = 0$, extending from the MS interface to the Ohmic contact. In order to fully simulate the 3-D structure from the 2-D mesh, the mesh points are appropriately weighted by their radial distance, ρ, from the $\rho = 0$ mesh boundary. A schematic of the mesh structure and its location with respect to the full contact structure is shown in Fig. 1(a), while a portion from an actual mesh, typical of those used in the simulations of MS contacts with cylindrical symmetry, is shown in Fig. 2. Typically, a grid consisting of over 1500 mesh points was used for each simulation. Because the Poisson and continuity equations are solved at each mesh point, the grid was improved by refining the mesh spacing in those regions for which there is large curvature in the potential and/or carrier concentration. As a result, the vertical mesh spacing is finest near the MS interface and the lateral mesh spacing is finest near the boundary region between the high SBH and low SBH contacts. The smallest mesh dimension was limited to about 5 Å. A gap of 5 Å in width (i.e., an annulus of 5 Å in thickness for the cylindrical geometry) was maintained between the high and low SBH regions at the MS interface in all of the simulations. The 5-Å dimension of the gap was small enough that it had no discernible effect on the numerical simulations, and a reduction in the gap width did not cause any noticeable change in the simulated potential and current distributions.

The second primary geometry which was considered in the simulations was a geometry consisting of low-SBH strips of infinite length and with width, L_0, and a SBH of $\Phi_B^0 - \Delta$ surrounded by a region of higher SBH, Φ_B^0 [see Fig. 1(b)]. Because of the infinite length of the strips and the surrounding region, the simulation region is truly two-dimensional. In addition, because of the Neumann boundary condition imposed at the lateral mesh boundaries, the simulated geometry may be considered to be a slice out of an infinitely repeating structure in the x direction with a period equal to twice the width of the mesh used in the simulations. Therefore, to simulate a low-SBH strip of width, L_0, surrounded by a higher SBH region, a mesh extending from the midpoint of the low-SBH strip ($x = 0$) to the high SBH region and with a length defined by the total device depth (taken to be greater than twice the depletion width) was used. The physical appearance of the mesh used in the simulation of the low-SBH strip is essentially identical to that shown in Fig. 2 for the cylindrical geometry. As in the case of the cylindrical geometry, a gap of 5 Å in width at the MS interface was maintained between the high-SBH and low-SBH regions.

For both the cylindrical and strip geometries, the low-SBH contact, the high-SBH contact, and the back Ohmic contact were defined independently. This enables the potential and current flow at each contact to be monitored independently. For all simulations, however, the bias was only applied at the Ohmic contact, and there was no potential difference between the high and low SBH contacts.

III. POTENTIAL DISTRIBUTION WITH SBH INHOMOGENEITY

A. The pinch-off effect

In this section, and the sections that follow, the potential distribution will be taken to be the potential of the conduction-band minimum (CBM) of the semiconductor and SBH inhomogeneity will refer to the spatial variation of the semiconductor CBM both with respect to the metal FL at the MS interface. Numerical simulations of uniform MS contacts for which there was no Schottky barrier inhomogeneity revealed potential distributions in good agreement with the accepted approximate 1-D theory.[5] Numerical simulations of spatially inhomogeneous MS contacts, however, revealed more complex behavior. Specifically, the primary geometry which was considered was that of a circular region of lower SBH embedded in a region of higher SBH. Intuitively, one may expect that this may be the most interesting geometry to consider (certainly, for the reverse geometry of small patches of high barrier height embedded in large regions of low SBH, it would be expected that current transport across the MS contact would be little affected by the high SBH patches). Details of the mesh and boundary conditions have been described earlier. For this simulation, and the simulations that follow, the semiconductor is assumed to be n-type silicon, unless otherwise noted. The other characteristics of the MS contact are included with the figures. Occasionally, the potential distribution was also calculated for a narrow low-SBH strip

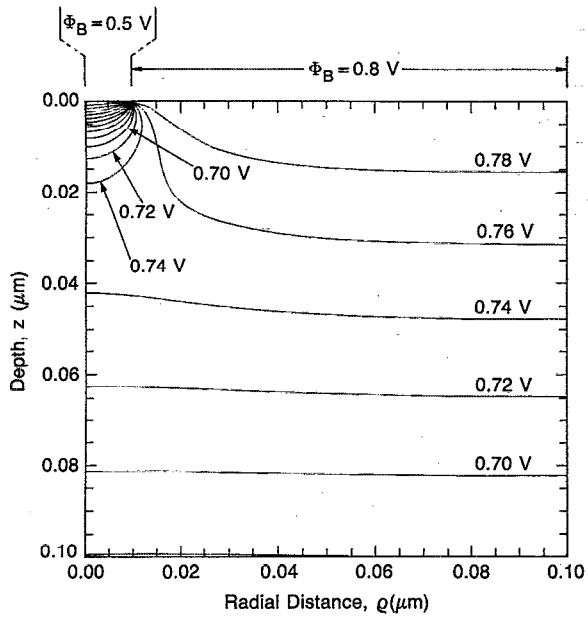

FIG. 3. Numerically determined potential contours at zero applied bias along a slice of constant azimuthal angle for a diode with cylindrical symmetry. The semiconductor is assumed to be n-type Si with doping 1×10^{15} cm^{-3}. The SBH of the high barrier region, Φ_B^0, is 0.8 V and the SBH of the low-SBH patch, $R_0 = 0.01$ μm, is 0.5 V ($\Delta = 0.3$ V). The simulation temperature is 300 K.

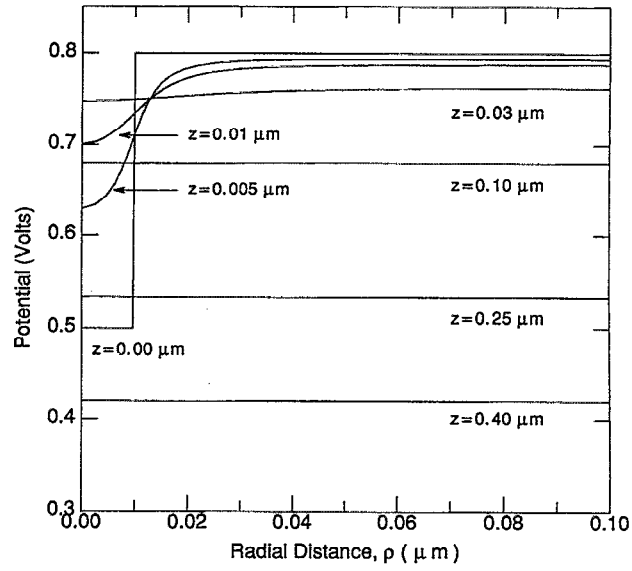

FIG. 4. Numerically determined potential contours parallel to the MS interface and at various depths in the semiconductor for the same MS contact as that shown in Fig. 3. The phenomenon of pinch-off of the low-SBH patch is clearly shown.

sandwiched between high-SBH regions with the geometry and mesh characteristics described earlier.

We begin our discussion of the potential at an inhomogeneous SB with an example. A circular patch with a radius, $R_0 = 0.01$ μm, and a SBH of 0.5 V was surrounded by an annulus with an outer radius of 0.1 μm and a SBH of 0.8 V. A gap of 5 Å was maintained between the inside low SBH patch and the outside high SBH region. Figure 3 is an enlargement of a potential contour plot along a fixed azimuthal angle extending from the center of the low-SBH patch ($\rho = 0$) to the outer edge of the high SBH annulus ($\rho = 0.1$ μm) and from the MS interface ($z = 0$) to a depth of $z = 0.1$ μm, about 1/8 of the way toward the edge of the depletion region. Careful examination of Fig. 3 will reveal a couple of features not observed with uniform MS contacts. First, the potential in the semiconductor directly beneath the low-SBH patch increases with increasing distance from the MS interface, reaches a maximum (at $z \approx 0.03$ μm), and then slowly decreases to the bulk value far from the MS interface. Beneath the high SBH regions, however, the potential decreases monotonically from the MS interface, similar to the behavior expected for uniform MS contacts. Another feature revealed in Fig. 3 is that the potential maximum along the $\rho = 0$ line is actually a saddle point. The potential increases from this point along directions parallel to the interface. The creation of a saddle point is a result of potential pinch-off. In this case, pinch-off refers to the blocking of the low barrier channel from the low-SBH contact into the semiconductor by the high potential of the surrounding high-barrier region.

Figure 4 is another view of the potential contours shown in Fig. 3, except the magnitude of the potential is shown explicitly at various depths within the semiconductor. The phenomenon of pinch-off is clearly evident in this figure. At the MS interface ($z = 0$), the potential contours are given by the chosen boundary condition of a patch of low SBH amidst a region of higher SBH. As z increases,

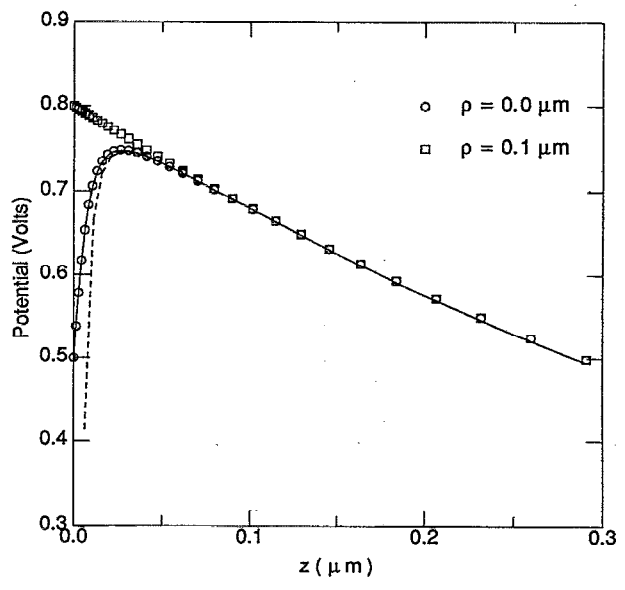

FIG. 5. Numerically determined potential distribution along a line normal to the MS interface and at the mesh boundary beneath the high barrier region, $\rho = 0.1$ μm, (shown as the squares) and beneath the center of the low-SBH patch, $\rho = 0$, (shown as the circles) for the same MS contact as shown in Fig. 3. The solid line is the potential distribution based on the analytic theory assuming a dipole layer at the MS interface, while the dashed line is the potential distribution based on the analytic theory which assumes a point dipole at the MS interface.

the disparity between potentials at different ρ's quickly damps out. This smoothing of potential leads to pinch-off. In Fig. 5 two potential contours along the z direction are shown for the same inhomogeneous MS contact. The squares mark the numerically simulated potential along a line normal to the MS interface at the far mesh boundary beneath the high SBH region ($\rho = 0.1$ μm). The circles mark the numerically simulated potential along the central axis ($\rho = 0$) of the low-SBH circular patch. This figure graphically displays that pinch-off of the low SBH region occurs some distance into the semiconductor. Note that outside the pinch-off region, the potential contours beneath the low and high SBH regions are essentially equal. It is apparent, at least for this choice of low-SBH patch dimensions and geometry, that the potential contours far from the MS interface are almost identical to the potential contours expected for a uniform patch with the same barrier height as the high barrier region. Therefore, for relatively small low-SBH patches, the depletion width boundary does not vary spatially and is quite similar to the depletion width boundary for a uniform MS contact. The dashed and solid lines in Fig. 5 are the predicted potential distributions based on the analytic theory of SBH inhomogeneity [Eqs. (A1) and (A5) in the Appendix].

B. Influence of low-SBH patch characteristics on the potential distribution

In order to determine how the potential near the interface of a MS contact with SBH inhomogeneity depends on the parameters of the inhomogeneity, we have performed numerical simulations as a function of the low-SBH patch size, the low-SBH patch geometry, the magnitude of the SBH difference, the substrate doping, the temperature, and the bias across the contact. All of these parameters were found to have an effect on the potential distribution near the MS interface. Since an analytic theory made definite predictions regarding the influence of these parameters on the potential distribution for inhomogeneous MS contacts, comparison will also be made with the analytic theory of SBH inhomogeneity.

1. Dependence on patch size

The potential distribution along the axis ($\rho = 0$) of circular patches with SBH of 0.4 V amidst regions with higher SBH of 0.8 V is shown in Fig. 6(a) for different patch radii, R_0. The circles are the numerical simulations based on PADRE while the solid lines are the solutions to the potential distribution from an analytic theory of SBH inhomogeneity, Eq. (A1). It is evident from the plots that as the low-SBH patch radius decreases, the patches become more pinched-off (i.e., the potential at the saddle point increases). At some critical patch size, there is no pinch-off, and for patches much larger than the critical size, the potential distribution approaches that of a uniform MS contact with the same SBH as that of the low-SBH patch. In this limit, the parallel conduction model espoused by Ohdomari and Tu is valid.[17] For the parameters chosen in Fig. 6(a), the critical patch radius is about 0.05 μm. This compares favorably with the critical patch radius of 0.047

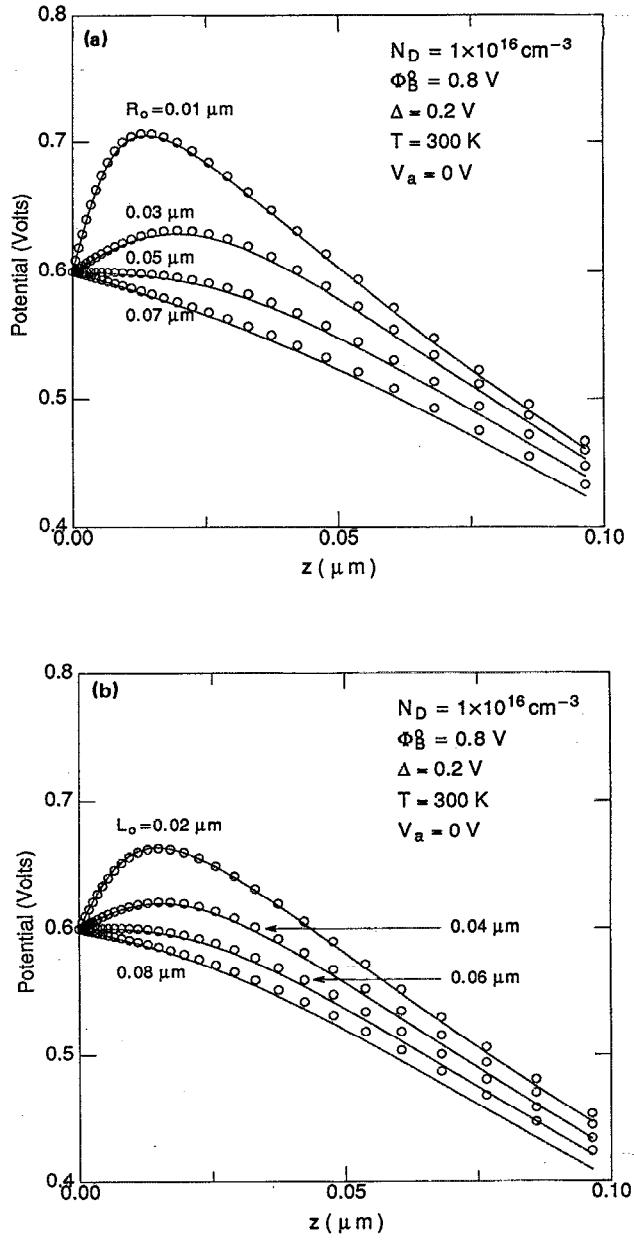

FIG. 6. Numerically determined potential distribution (shown as circles) along $\rho = 0$ or $x = 0$ of the low-SBH region for various low-SBH radii or strip widths: (a) cylindrical geometry, (b) strip geometry. The potential based on the analytic theory is shown as the solid lines.

μm calculated on the basis of the analytic theory, Eq. (A3). In Table I, we show the critical patch radii for different doping levels and SBH differences, Δ, as determined through numerical simulations and how they compare with the critical radii calculated from the analytic theory. In Fig. 6(b) we show how the potential distribution varies when the SBH inhomogeneity is in the form of strips of low SBH with a width, L_0 and of infinite length. This geometry is the strip geometry discussed earlier. Similarly to the circular patch geometry, there is a critical low-SBH strip width below which the potential at the center of the low-SBH strip is pinched-off. From the figure, the critical strip width may be estimated to be about 0.06 μm, which is in

TABLE I. Critical radius, $R_{0,crit}$, for a circular low-SBH patch surrounded by a high SBH region at zero bias and 300 K. Pinch-off of the low-SBH patch only occurs when the patch radius is less than $R_{0,crit}$.

N_D (cm^{-3})	Φ_{B0} (V)	Δ (V)	$R_{0,crit}$ (μm) from simulations	$R_{0,crit}$ (μm) from analytic theory
1×10^{15}	0.8	0.2	$0.14 < R_{0,crit} < 0.17$	0.16
		0.4	$0.33 < R_{0,crit} < 0.37$	0.31
1×10^{16}	0.8	0.2	$0.04 < R_{0,crit} < 0.05$	0.047
		0.4	$0.09 < R_{0,crit} < 0.10$	0.094
1×10^{17}	0.8	0.2	$0.012 < R_{0,crit} < 0.016$	0.014
		0.4	$0.026 < R_{0,crit} < 0.030$	0.028

very good agreement with the value of 0.060 μm predicted from the analytic theory, Eq. (A4).

2. Dependence on SBH difference

In Fig. 7, the potential distributions along $\rho = 0$ of low-SBH circular patches are plotted for patches with different Δ's. Again, the circles represent the potential obtained from numerical simulations based on PADRE, while the solid lines are the predicted potential distributions based on the analytic theory of SBH inhomogeneity [Eq. (A1)]. When Δ is less than some critical value, there is no potential pinch-off. This is similar to the situation shown in Fig. 6 in which there is a critical radius for pinch-off. The larger Δ is, the greater is the degree of pinch-off. Of course, as Δ approaches zero, the potential profiles become identical to those of a MS contact with uniform SBH. From the figure, we estimate that the critical Δ for potential pinch-off is about 0.09 V, for the particular parameters chosen. This compares favorably with the value of 0.090 V predicted from the analytic theory [Eq. (A3)]. In Table II, we show the critical Δ's determined through numerical simulations for a range of doping levels and two low-SBH patch radii. Again, good agreement is found with the predictions of the analytic theory.

3. Dependence on substrate doping

In Fig. 8, the potential distributions along $\rho = 0$ of a circular patch of low SBH are shown as a function of the substrate doping level. The circles are the results from the numerical simulations and the lines are from the analytic theory. When the substrate doping is low, the magnitude of the potential at the saddle point is high, and, hence, the low-SBH patch is more pinched-off. Alternatively, when the doping level is high enough, the low-SBH patch is no longer pinched-off. The dependence of the potential distribution on the substrate doping level may be understood qualitatively by comparison with the dependence of the potential distribution on the low-SBH patch dimensions at a constant substrate doping level (see Fig. 6). The important parameter is the low-SBH patch dimension scaled by the semiconductor depletion width. As the doping level decreases, the depletion width becomes much larger than the low-SBH patch radius, and the potential in the vicinity of the low-SBH patch becomes more pinched-off. When the doping level increases, the depletion width becomes small compared to the low-SBH patch radius and the potential is no longer pinched-off. This shows that the degree of SBH fluctuation is always significantly reduced on lightly doped semiconductors. Conversely, the most information about SBH inhomogeneity may be obtained from heavily doped semiconductors.

4. Dependence on temperature

The temperature dependence of the potential distribution in the vicinity of a circular patch of low SBH along $\rho = 0$ is shown in Fig. 9. The overall temperature dependence of the potential distribution is weak. However, there is a noticeable increase in the magnitude of the potential at the saddle point with temperature, arising from a weak temperature dependence of the Fermi potential, V_n. In addition, at higher temperatures, the increased carrier density in the space-charge region leads to a net charge density which is smaller than N_D, thus increasing the apparent depletion width. The neglect of the increased carrier density in the depletion region is a drawback of the analytic theory and is the reason for the slight disagreement, at

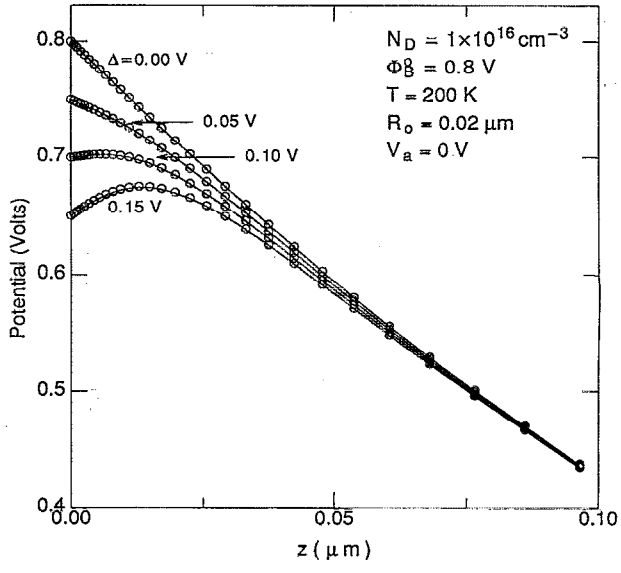

FIG. 7. Numerically simulated potential distribution (shown as circles) along $\rho = 0$ of the low-SBH patch for various Δ's. The potential based on the analytic theory is shown as the solid lines.

TABLE II. Critical difference in SBH between the low- and high-SBH regions, Δ_{crit}, at zero bias and 300 K. Pinch-off of the low-SBH patch only occurs when Δ is larger than Δ_{crit}.

N_D (cm^{-3})	$\Phi_{B,0}$ (V)	R_0 (μm)	Δ_{crit} (V) from simulations	Δ_{crit} (V) from analytic theory
1×10^{15}	0.8	0.03	$0.03<\Delta_{crit}<0.05$	0.038
		0.10	$0.10<\Delta_{crit}<0.15$	0.13
1×10^{16}	0.8	0.03	$0.10<\Delta_{crit}<0.15$	0.14
		0.10	$0.40<\Delta_{crit}<0.45$	0.43
1×10^{17}	0.8	0.03	$0.35<\Delta_{crit}<0.45$	0.47
		0.10	$0.8<\Delta_{crit}$	no pinch-off

large z, between the numerically simulated potential distribution and that based on the analytic theory [Eq. (A1)].

5. Dependence on bias

In Fig. 10(a), the potential distributions along $\rho = 0$ of a circular patch of low SBH are shown for different voltage biases across the MS contact. It is evident from the plot that the potential at the saddle point increases with increasing forward bias and decreases with reverse bias. Note that the variation in the magnitude of the potential at the saddle point is not linearly proportional to the applied bias. There is a large change in the potential at the saddle point for a given forward bias than for the equivalent amount of reverse bias. The analytic theory predicts that the bias dependence of the saddle point potential should be proportional to the 1/3 power of the band bending, V_{bb} [Eq. (A6)]. In Fig. 11, we test this prediction in a plot of the saddle point potential as a function of $V_{bb}^{1/3}$. Note that the linear relationship predicted by the analytic theory is supported by the numerical simulations. The analytic theory predicts a slightly larger bias dependence of the saddle point potential than is observed numerically. The discrepancy most likely arises from the point dipole approximation of the analytic theory, which does not perfectly describe the potential distribution near large low-SBH patches. Even though the total change in the magnitude of the potential at the saddle point is only a small fraction of the change in the applied bias, this change has important implications for mechanisms of current transport across the MS contact. When the pinch-off of the low-SBH region is small relative to the magnitude of the SBH, the total current through the MS contact at forward bias may be dominated by the current through the region of low SBH. Since the effective barrier height of the low-SBH region is given by the magnitude of the potential at the saddle point, a variation in the potential at the saddle point with bias implies a variation in effective SBH with bias. This dependence on bias has significant consequences in the determination of ideality factors and the soft reverse characteristics of real MS contacts, to be discussed later. Figure 10(b) is a similar plot to Fig. 10(a) except that the semiconduc-

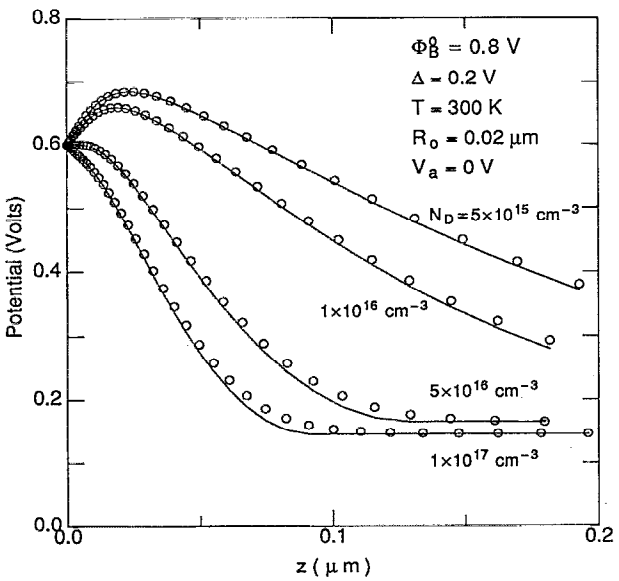

FIG. 8. Numerically simulated potential distribution (shown as circles) along $\rho = 0$ of the low-SBH patch for various n-type substrate doping levels. The potential based on the analytic theory is shown as the solid lines.

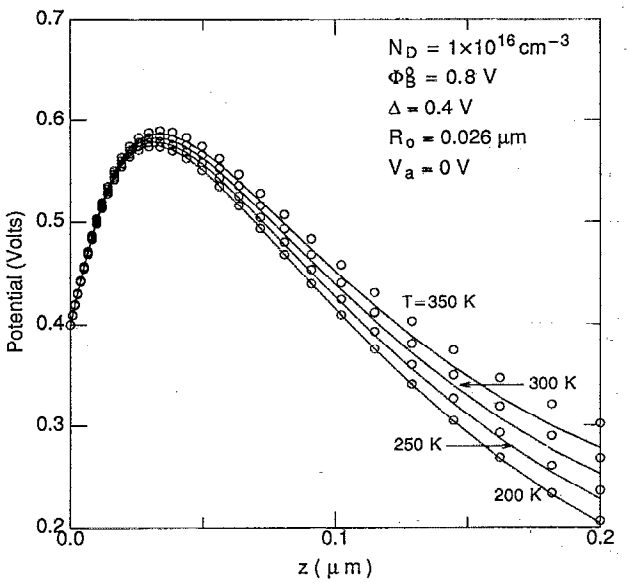

FIG. 9. Numerically simulated potential distribution (shown as circles) along $\rho = 0$ of the low-SBH patch for various temperatures. The potential based on the analytic theory is shown as the solid lines.

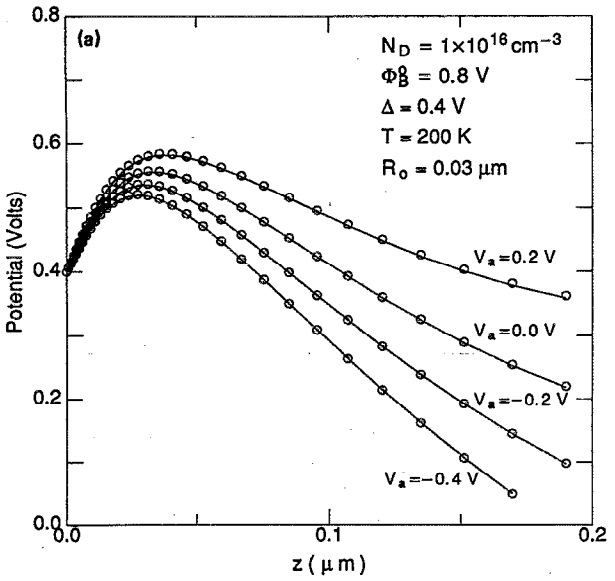

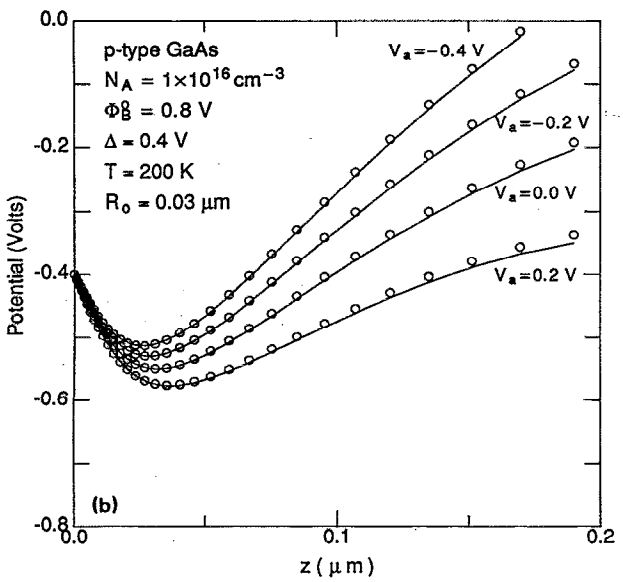

FIG. 10. (a) Numerically simulated potential distribution (shown as circles) along $\rho = 0$ of the low-SBH patch at different biases across the MS contact. The potential based on the analytic theory is shown as the solid lines. (b) Same as (a), except here the semiconductor is simulated to be p-type GaAs and the potential is the valence-band maximum.

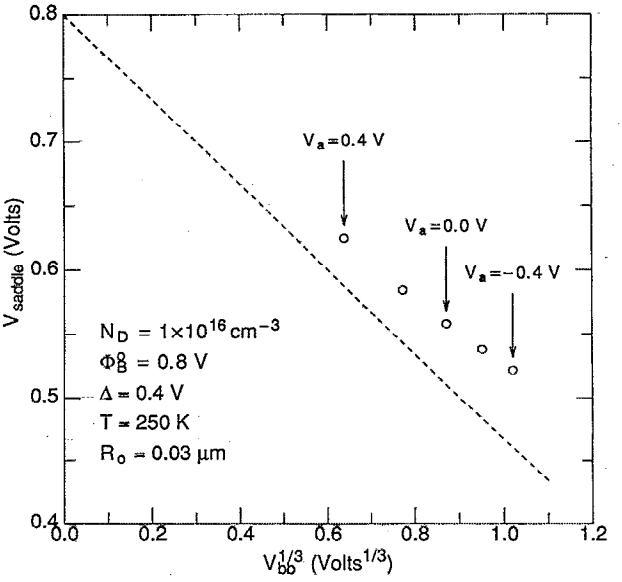

FIG. 11. Saddle point potential plotted as a function of the 1/3 power of the band-bending potential, V_{bb}. The dashed line is the expected dependence based on the analytic theory.

tor was replaced with p-type GaAs in the simulations. Since the origins of pinch-off are not dependent on the nature of the semiconductor involved, the type of the majority carrier in the semiconductor, or the gross geometry of the inhomogeneity, it is natural to expect that simulations involving semiconductors other than Si, with p-type semiconductors rather than n-type, and with geometries in which the low-SBH region is in the form of strips or narrow channels, should exhibit the same characteristic behavior of pinch-off that is observed for n-type Si with circular patches of low SBH. Figure 10(b) is just one indicator of the general validity of this statement.

6. Dependence on position

The pinch-off of the low-SBH patches is dependent on neighboring regions of higher SBH. When the region of higher SBH surrounding the low-SBH region is diminished in area, the low-SBH region is less pinched-off. Typical MS contacts are large enough (with dimensions orders of magnitude larger than the semiconductor depletion width) that low-SBH patches located away from the contact edges may be appropriately simulated by patches which are surrounded by an essentially infinite region of higher SBH. Closer to the edges of the contact, however, there is progressively less high-SBH contact area along at least one edge of the low-SBH region, and this affects the pinch-off of these regions. In order to demonstrate this effect, in Fig. 12 we show numerical simulations of the potential distribution near a region of low SBH when that region is located at various distances from the edge of the MS contact. A strip geometry was used in which a strip of low SBH with a width of 0.02 μm and a SBH of 0.4 V was surrounded by strips of higher SBH, 0.8 V, and a contact-free region was included. The geometry of the simulations is similar to that shown in Fig. 1 for the strip geometry, except that the left mesh boundary now occurs in a region of high SBH and the right mesh boundary occurs in a contact-free region, with the low-SBH strip appearing between these boundaries. In the simulations, the position of the low-SBH strip with respect to the MS contact edge was varied, keeping the total area of the low-SBH strip and high-SBH strips constant. In Fig. 12(a), potential contours along a 2-D slice through the MS contact are shown for the situation in which the low-SBH strip was placed farthest from the contact edge. The low-SBH strip is clearly pinched-off, with the saddle point potential being approximately 0.59 V. Figure 12(b) shows the potential distribu-

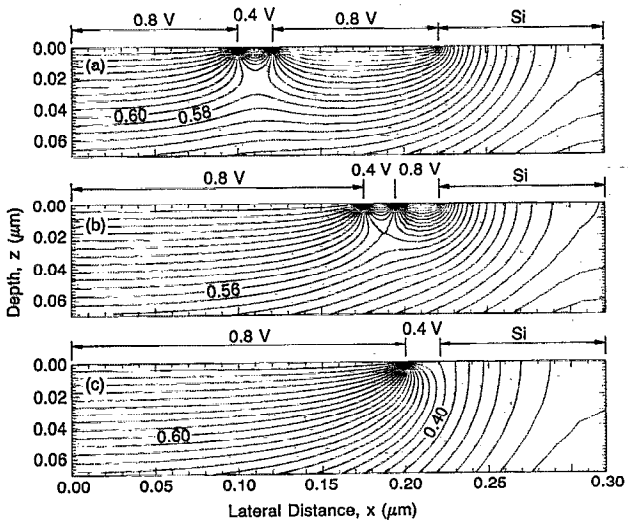

FIG. 12. Two-dimensional potential contours of a MS contact with the strip geometry in which a low-SBH strip is placed at various distances from the contact edge. The high-SBH region has a SBH of 0.8 V while the low-SBH strip, 0.02 μm in width, has a SBH of 0.4 V. The substrate is n-type Si with a doping of 1×10^{16} cm^{-3} and the simulation temperature is 250 K. (a) farthest from the contact edge, (c) low-SBH strip at the contact edge. Pinch-off of the low-SBH strip decreases the nearer the strip is to the contact edge.

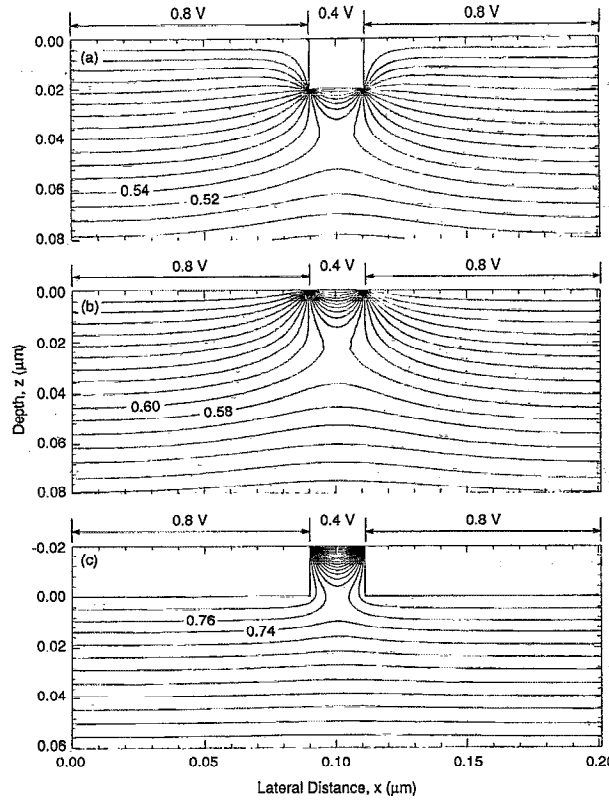

FIG. 13. Two-dimensional potential contours of a MS contact with the strip geometry in which a low-SBH strip is positioned at various distances from the high-SBH MS interface plane. The high-SBH region has a SBH of 0.8 V while the low-SBH strip, 0.02 μm in width, has a SBH of 0.4 V. The SBH of the sidewalls neighboring the low-SBH strip in (a) and (c) is assigned to be 0.8 V. The substrate is n-type Si with a doping of 1×10^{16} cm^{-3} and the simulation temperature is 250 K. (a) low-SBH strip located in a trench in the semiconductor, (b) planar interface, and (c) low-SBH strip located on a ridge protruding from the MS interface. Pinch-off of the low-SBH strip is least for (a).

tion when the low-SBH strip is moved closer to the contact edge, and in Fig. 12(c) the potential contours are shown when the low-SBH strip is placed right at the edge of the contact. As the low-SBH strip is moved closer to the contact edge, the strip becomes progressively less pinched-off, i.e., the potential at the saddle point decreases. This effect is a direct result of the reduced high-SBH region near the diode edge. In Fig. 12(b), it is also apparent that the saddle point does not occur directly beneath the low-SBH strip, rather it is skewed towards the diode edge, the direction in which the high-SBH area has been diminished. When the low-SBH strip is immediately adjacent to the diode edge, Fig. 12(c), there is, in fact, no saddle point. The potential decreases continuously from the edge of the low-SBH strip along the contact-free surface. As may be imagined, this reduction in the saddle point potential or elimination of the saddle point may significantly influence the current transport across the inhomogeneous MS contact. More will be discussed about this point later.

7. Dependence on interface planarity

Interface nonplanarity may seriously affect pinch-off of low-SBH patches. A region of low SBH extending into the semiconductor will be less pinched-off than a corresponding region of low SBH at a planar interface. Similarly, a protrusion of a region of low SBH away from the MS interface will be more pinched-off. The explanation for the reduced or enhanced pinch-off at nonplanar interfaces is the same as that for the reduction in pinch-off near contact edges. The pinch-off of the low-SBH region is influenced by the proximity of regions of higher SBH. Moving the low-SBH region away from the MS interface and into the semiconductor effectively reduces the influence of the neighboring high SBH regions, thus resulting in decreased pinch-off. A similar argument explains the enhanced pinch-off of the low-SBH region protruding from the MS interface. Numerical simulations of the influence of interface planarity on the pinch-off of low-SBH patches are shown in Fig. 13. A strip of SBH of 0.4 V, 0.02 μm in width, is positioned between regions of higher SBH, 0.8 V, with a geometry similar to that of Fig. 12, except a nonplanar interface is assumed and there is no contact edge. For the trench and ridge geometries, the side walls neighboring the low SBH region is assigned a high SBH of 0.8 V. In Fig. 13(a), the low-SBH strip is located in a trench of depth 0.02 μm into the semiconductor. Potential contours at zero bias are shown for a region around the low-SBH strip and extending to a depth of 0.08 μm into the semiconductor. In Fig. 13(b), the low-SBH strip is located between regions of higher SBH at a planar interface. In Fig. 13(c), the low-SBH strip is located as a ridge protruding away from the semiconductor with a height of 0.02 μm. It is clear from the potential contours that the magnitude of the potential at the saddle point (which determines the degree of pinch-

off) is least for the low-SBH strip located in a trench into the semiconductor (about 0.53 V) and is greatest for the low-SBH strip located on a ridge (about 0.75 V). These results are completely consistent with the above discussion.

8. Dependence on the reduced patch characteristic, γ

Guided by the predictions of the analytic theory for SBH inhomogeneity, we expect the potential distribution, away from the MS interface, to be similar when the factor, γ, the temperature, and substrate doping are constant [Eqs. (A6) and (A7)]. As a test of the assumed invariance of the potential contours, numerical simulations were carried out for three different patches with different R_0's and different Δ's, but identical γ's. These simulations are overlaid in Fig. 14, where the input profiles ($z = 0$) are also shown. As is shown in the plot, even though there is a large variation in Δ and a corresponding variation in R_0, the potential contours at the saddle point are all quite similar. Hence, it should be sufficient to investigate the potential distribution and current transport through inhomogeneous contacts as a function of this factor, γ, rather than numerically simulating all possible patch dimensions and Δ's, etc. It is for this reason that γ is a useful parameter to describe SBH inhomogeneity. However, since the concept of a reduced parameter, γ, is linked to the point dipole approximation assumed in the analytic theory, it is valid only when R_0 is small compared with W. At large γ's, which necessarily involve large R_0's, the point dipole approach becomes a poor approximation of the actual situation. Therefore, even though γ is a useful parameter which describes small low-SBH patches very accurately, it is not suited for large low-SBH patches (large γ's).

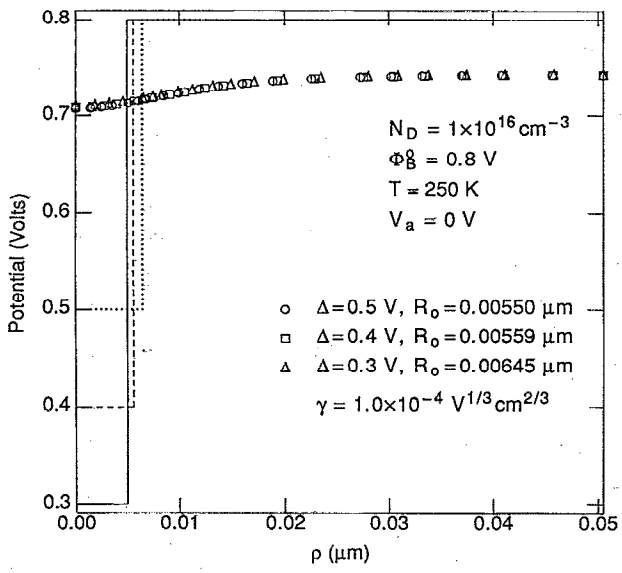

FIG. 14. Numerically simulated potential distribution at the MS interface (solid, dashed, and dotted lines) and at the position of the saddle point along a line parallel to the MS interface for three different patches characterized by the same γ value.

C. Scaling of the potential distribution

The numerical simulations so far have shown that when there are small regions of low SBH amidst regions of higher SBH, the potential contours beneath the low-SBH regions are pinched-off. This pinch-off is a function of the size of the low-SBH region, the magnitudes of the two SBH's, the substrate doping, the temperature, and the bias across the MS contact. Since the potential is a complicated function of many variables, we looked for systematics in the saddle point potential for a possible reduction in the number of variables which are truly independent. Although the trends are clear, namely, an increase in patch dimensions decreases the pinch-off, a decrease in Δ decreases the pinch-off, and forward bias increases the potential at the saddle point, while reverse bias has the opposite effect, it is inconvenient to use the numerical simulations alone to estimate, for arbitrary patch dimensions, Δ, bias, etc., what the potential distribution within the semiconductor will look like. One of the most important predictions of the analytic theory is that the natural scales for the potential distribution is the semiconductor depletion width, W, and the band bending, V_{bb}. If length scales are normalized by W and potentials are normalized by V_{bb}, then there exists a single parameter which may be used to describe the potential distribution. This parameter is dependent on the geometry of the SBH inhomogeneity. For the circular patch of low SBH, the parameter is defined as Γ [Eq. (A8)]. Therefore, when there exist circular patches of low SBH all characterized by the same factor, Γ, the potential distributions along the axis of the low-SBH patch should be identical for all patches, provided the length scale is normalized by W and the potential is normalized by V_{bb}. As a test of this prediction, Fig. 15(a) shows the absolute potential distributions along $\rho = 0$ for circular patches of low SBH with diode parameters given in Table III and all characterized by the same Γ. Figure 15(b) shows the normalized potential distributions in which the length scale has been normalized by W and the potential has been normalized by V_{bb}. When the potential distribution is scaled in this manner, the three curves are indistinguishable. From this, we can conclude that the relevant parameters which control the scaling of the potential distribution in the presence of SBH inhomogeneity are, indeed, the depletion width and the band bending. The depletion width is a function of the semiconductor doping level, the permittivity of the semiconductor, and the band bending. The band bending is a function of the semiconductor doping level, temperature, the barrier height, and bias. It is the interplay of these parameters which results in the potential distributions shown in the numerical simulations. Although there are a large number of parameters, it is only necessary to know the Γ of the low-SBH patch to get a complete picture of the potential distribution.

At this point, it is useful to reiterate some of the conclusions which can be drawn from looking at the potential distribution within the semiconductor when there is a spatial variation of the SBH at the MS interface. The most significant point is that regions of low SBH which are comparable in size to the semiconductor depletion width are

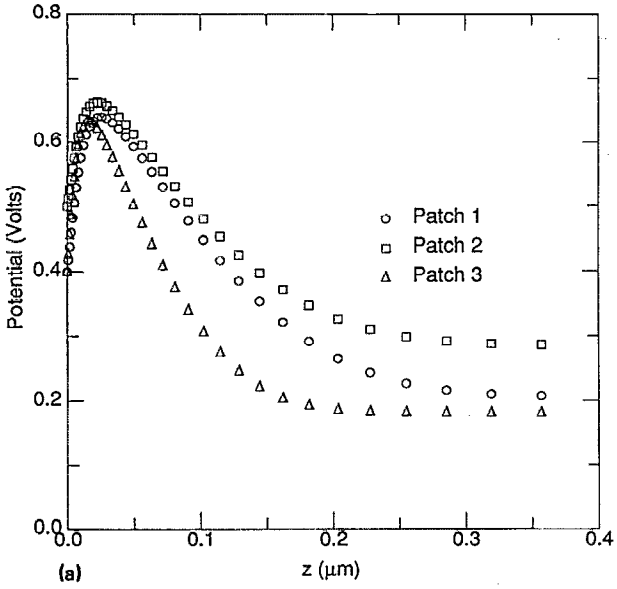

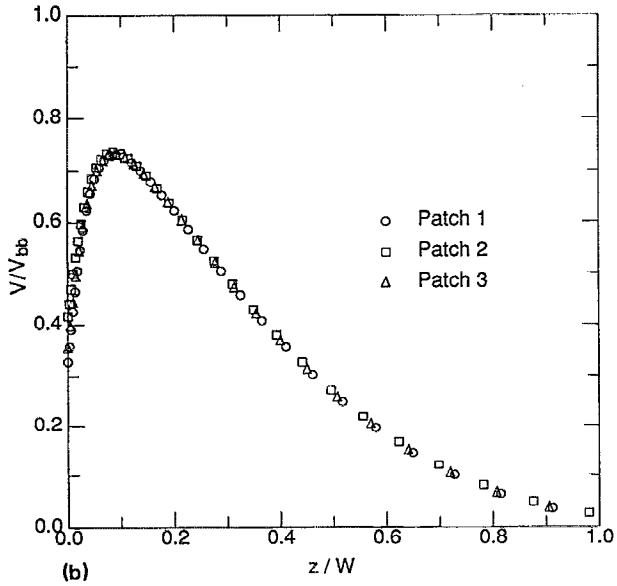

FIG. 15. Potential distribution along $\rho = 0$ of low-SBH patches for three different patches of different size, doping, temperature, bias, but all characterized by the same value of Γ: (a) unscaled potential distribution, (b) potential distribution with the potential scaled by V_{bb} and distance scaled by W.

frequently pinched-off. Hence probes which are sensitive to the transport of carriers across the MS interface, i.e., I-V measurements, photoresponse measurements, ballistic electron emission microscopy (BEEM), electron beam induced current (EBIC), may tend to underestimate the degree of inhomogeneity at the MS interface. Pinch-off is especially significant when the substrate doping is low, so for maximum sensitivity to possible spatial variation in the interface SBH, it is most useful to use higher doped substrates.

IV. CURRENT TRANSPORT THROUGH AN ISOLATED REGION OF LOW SBH

Numerical simulations of current transport through inhomogeneous MS contacts allow an easy analysis of individual current components. In particular, if the MS contact consists of a region with low SBH and a region with higher SBH, by distinguishing between the current flow to the two regions, it is possible to deduce, separately, the functional form of the current flows. Because of the complexity of real MS interfaces, such a break-down of the current into individual components is not possible experimentally. The magnitude of the numerically simulated junction current contains information on the potential barrier to electron transport. In practice, the determination of the effective barrier height requires some assumption to be made concerning the form of the transport mechanism for current flow across the MS contact.[6] To determine an effective barrier height for the low-SBH patch from the numerical simulations, we have assumed a transport behavior based on thermionic emission theory with an effective area, A_{eff}, given by the analytic theory, cf. Eqs. (A9) and (A12). We have determined the constant, A^*, through numerical simulations of uniform diodes and requiring that the measured effective SBH be equal to the SBH defined for the uniform diode. Although the value of A^* calculated from the numerical simulations of uniform diodes on n-type Si was found to be slightly temperature dependent, a constant A^* of 370 A cm^{-2} K^{-2} was assumed for the calculation of the absolute effective barrier heights of the low-SBH patches and the inhomogeneous diodes. Errors introduced by this uncertainty in A^* are small (in the worst case, the calculated effective barrier height changes by $<5\%$). Therefore, quantitative analyses of the current transport at inhomogeneous SBs by numerical simulations are valid.

As was done for the numerical simulations of the potential distribution of inhomogeneous MS contacts, we simulate a geometry in which there is a circular patch of low SBH amidst a uniform region of higher SBH on n-type Si. Carrier transport was simulated by simultaneously solving the Poisson and two carrier continuity equations as a function of bias across the MS contact. Concentration dependent lifetimes and mobilities were assumed for the carriers. The current reaching the low-SBH region of the MS interface was recorded as a function of bias across the MS contact. An I-V plot was constructed based on the logarithm of the current as a function of applied voltage, which typically was varied by 25-mV increments. While the magnitude of the current flowing through the low-SBH region

TABLE III. Parameters of the low-SBH patches used to demonstrate the equivalence of the potential distribution for patches characterized by the same Γ value when the absolute potential is normalized by V_{bb} and the absolute dimension is normalized by the depletion width.

	Patch 1	Patch 2	Patch 3
$\Phi_{B,0}$ (V)	0.8	0.8	0.8
Δ (V)	0.4	0.3	0.4
N_D (cm^{-3})	1×10^{16}	1×10^{16}	2.534×10^{16}
Temperature (K)	300	300	300
R_0 (μm)	0.0153	0.0153	0.01
V_a (V)	0	0.0797	0
Γ	0.10	0.10	0.10

is dependent on the current transport model which was used in the simulation, the slope of the I-V plot should be independent of the current transport mechanism, provided the mechanism is based on drift-diffusion or thermionic emission. Therefore, the slope was determined by regression to linear regions of the numerically created I-V plot. It is more common to characterize the slope by determining the ideality factor, n, which is the inverse slope of the I-V plot, multiplied by β ($\beta = q/k_BT$).

A. Dependence of current transport on the low-SBH patch characteristics

1. Dependence on γ

The ideality factor is expected to be close to 1.00 based on drift-diffusion or thermionic emission current transport theories. Indeed, the ideality factor determined from numerical simulations of the current flow across uniform MS contacts was found to be very close to unity (typically <1.03). However, current transport through inhomogeneous SBs was found to be characterized by ideality factors which deviate significantly from unity. The physical origin behind the dependence of the ideality factor on SBH inhomogeneity may be easily understood based on the discussion of the potential distribution in the previous section. Since carrier transport mechanisms across the MS interface, excluding tunneling mechanisms, depend exponentially on the barrier height, a higher fraction of the total current will flow through the region of semiconductor near the saddle point, hence the effective local barrier height will be defined by the saddle point potential. Since the height of the saddle point changes as a function of bias, the apparent barrier height changes, and this bias-dependence of the barrier height gives rise to the ideality factor in excess of unity. Note that the imposition of SBH inhomogeneity also directly results in a nonuniform current density in the semiconductor. Numerical simulations may be used to quantify the dependence of the ideality factor on inhomogeneity because currents flowing to different regions of the MS interface can be analyzed separately.

Currents flowing in high-SBH regions of inhomogeneous MS contacts have ideality factors close to unity, similar to that observed at uniform SB diodes. The components of current flowing in low-SBH patches, however, shows more complicated dependence on bias. Numerical simulations show n depends on R_0 and Δ. However, these dependences may be reduced to a single dependence on γ. In order to correlate the ideality factor with SBH inhomogeneity, we have plotted in Fig. 16(a) the ideality factors determined by numerical simulation of the current flow through regions of low SBH as a function of γ, the generalized inhomogeneity factor mentioned earlier. The dashed line is the predicted dependence of the ideality factor on γ based on the analytic model of SBH inhomogeneity, Eq. (A10). It is clear from the plot that a linear relationship describes well the dependence of the simulated ideality factor for the low-SBH patch on γ. This observation is very significant for it allows a quantification of the dependence of the ideality factor on SBH inhomogeneity, i.e., the larger the γ, the larger the ideality factor.

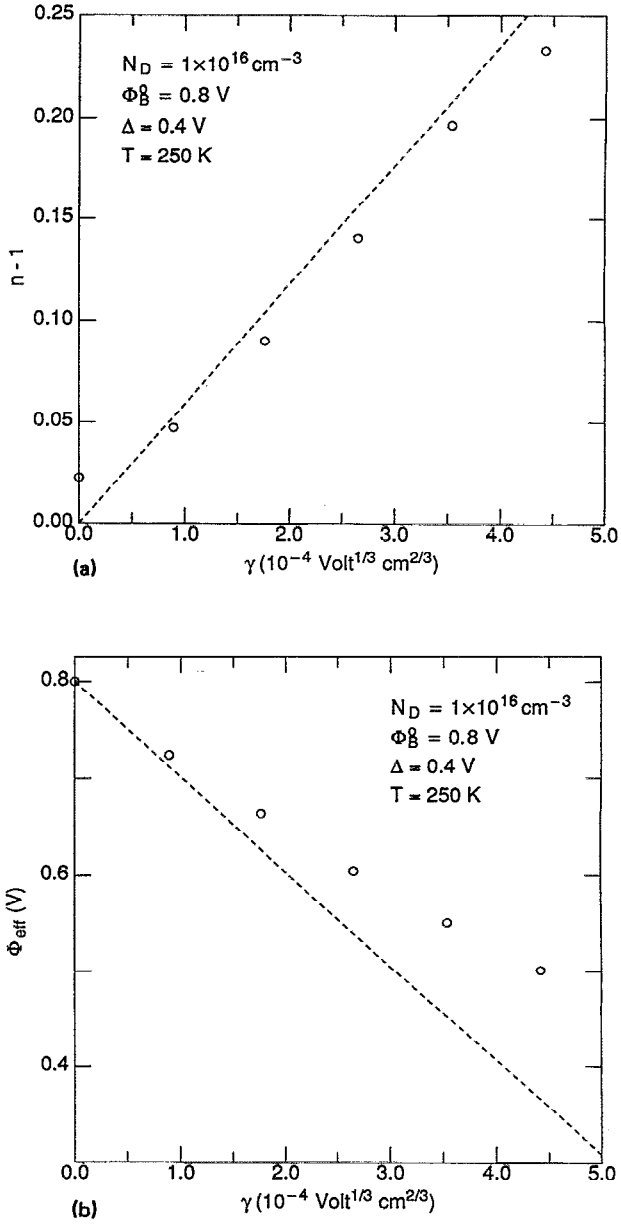

FIG. 16. Numerically determined variation of (a) the low-SBH patch ideality factor and (b) the low-SBH patch effective SBH with γ. The circles represent the points obtained from the numerical simulations, and the dashed line is the expected result based on the analytic theory.

The effective SBHs of the low-SBH patches seem to scale linearly with γ, as shown in Fig. 16(b). The dashed line represents the expected behavior based on the analytic theory. The correlation shown in Fig. 16(b) clearly shows that the larger the γ, the smaller the effective barrier height. This result is intuitively clear from the discussion in the previous section on the potential distributions. If γ is large (Δ is large and/or R_0 is large), then the saddle point, which determines the effective SBH, is lower. The numerical simulations have, in general, shown that the analytic theory is indeed adequate to explain current transport in the presence of SBH inhomogeneity. At low values of γ the agreement is almost perfect, while for larger γ values some deviations become apparent. The most significant reason

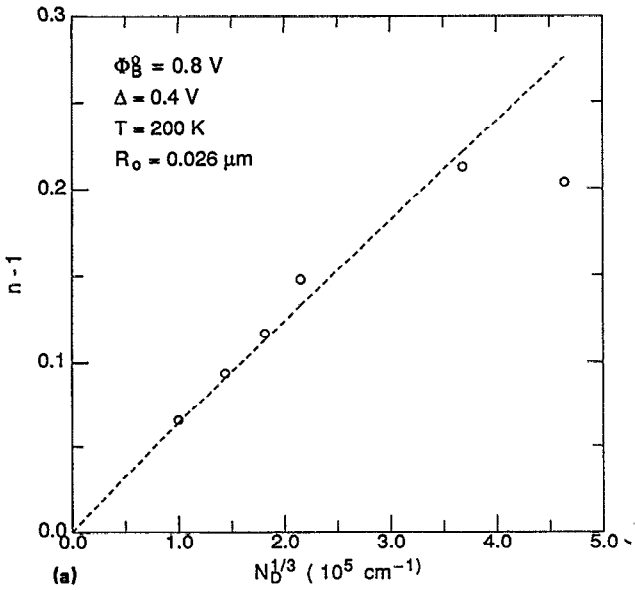

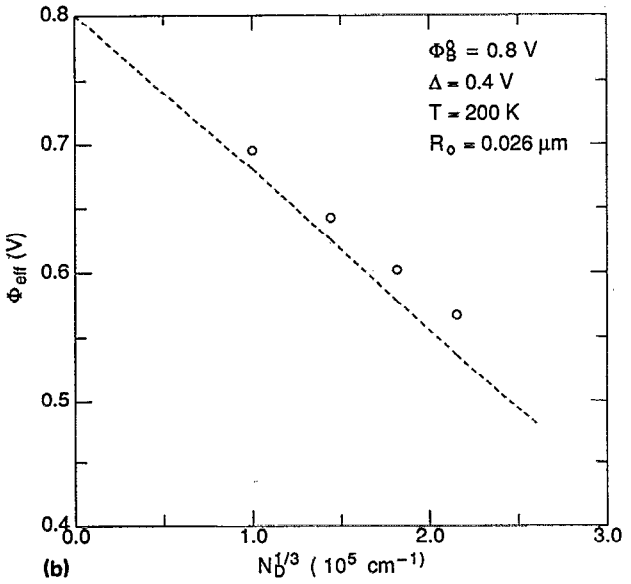

FIG. 17. Numerically determined variation of (a) the low-SBH patch ideality factor and (b) the low-SBH patch effective SBH with doping of the semiconductor. The circles represent the points obtained from the numerical simulations, and the dashed line is the expected result based on the analytic theory.

for the larger deviations for large γ's in Fig. 16 is that the analytic theory assumes the validity of the point dipole approximation in describing the potential contours for current flow across the MS contact. Nevertheless, the general form of the predicted dependence of the ideality factor and effective SBH on γ is well-supported by the numerical simulations.

2. Dependence on doping level

In Figs. 17(a) and 17(b), we show the dependence of the ideality factor and effective SBH for the low-SBH patch on doping of the substrate. In accordance with the analytic theory, in Fig. 17(a) we have plotted the ideality factor as

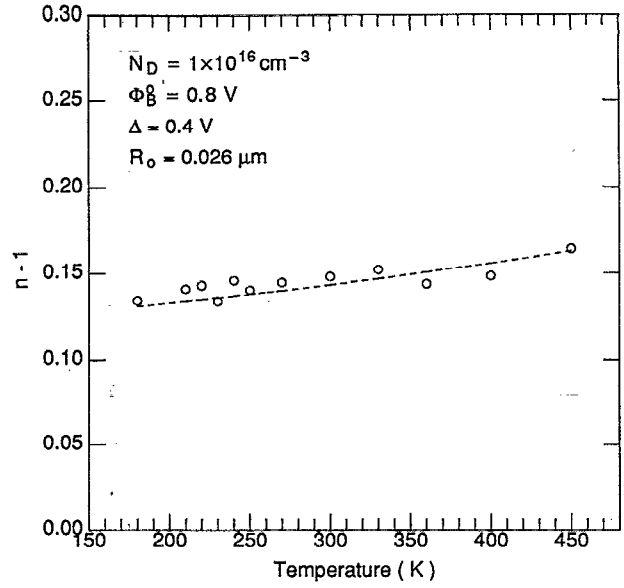

FIG. 18. Numerically determined variation of the low-SBH patch ideality factor with temperature. The circles represent the points obtained from the numerical simulations, and the dashed line is the expected result based on the analytic theory.

a function of the 1/3 power of the doping concentration, N_D [Eq. (A10)]. It is apparent from the plot that, at least for lightly doped semiconductors, the dependence of ideality factor on doping for this circular low-SBH patch geometry does seem to be proportional to the 1/3 power of the doping. The dashed line in Fig. 17(a) is the predicted behavior based on the analytic theory. At higher doping levels, W decreases and there is significant deviation from a $N_D^{1/3}$ dependence on doping. As shown in Fig. 17(a), even if there is appreciable SBH inhomogeneity for a given sample, as long as the semiconductor doping is low, the influence of this inhomogeneity will not be observed, i.e., the ideality factor will remain close to unity and the measured barrier height would be as expected for a uniform sample. In Fig. 17(b), we show the dependence of the effective barrier height of the low-SBH patch on $N_D^{1/3}$. The dashed line is the predicted dependence from the analytic theory [Eq. (A11)]. At lower doping levels, the agreement between the simulations and the analytic theory is excellent. At higher doping levels, there is some discrepancy which is related to the failure of the point dipole approximation of the analytic theory in describing the potential distribution near the region of the saddle point.

3. Dependence on temperature

In Fig. 18 we plot ideality factors for a low-SBH patch as a function of temperature. The dashed line is, again, the predicted behavior based on the analytic theory. The numerical simulations support the temperature dependence of the ideality factor for a low-SBH patch predicted from the analytic theory, Eq. (A10). The scatter in the ideality factors is most likely related to uncertainty in the determination of ideality factors through fitting of the numerically

created I-V plots. At high temperature, the current flow through the low-SBH patch is increased, and series resistance begins to seriously limit the linear range of the I-V plot. As a result, the ideality factor, determined by regression to this linear region, is less accurate. The significant point to be noted from this plot is that the ideality factor for the low-SBH patch is almost independent of temperature. If the total current through a MS contact was dominated by the current through one low-SBH patch, then the ideality factor determined for the entire MS contact would be essentially temperature-independent. Experimentally observed ideality factors, and SBHs, often show a strong dependence on temperature, seemingly in disagreement with the results presented so far for a single low-SBH patch. However, as explained in the next section, these experimentally observed dependences may result from MS contacts having an assortment of low-SBH patches with different γ's.

V. CURRENT TRANSPORT ACROSS REAL MS CONTACTS

Although the numerical simulation of the current flowing through the low-SBH patch is useful for understanding the relationship between the ideality factor and inhomogeneity, the experimental characterization of real MS contacts is based on the current which flows across the entire MS contact, typically with dimensions many orders of magnitude larger than the depletion width. It is impractical to directly simulate the I-V behavior of a macroscopic SB diode. However, a general idea of the current transport at a complex inhomogeneous SB diode may be obtained by studying the total sum, in different proportions, of individual current components simulated from isolated, smaller inhomogeneous SB diodes. Simulations based on this approach are used to understand various anomalous behavior frequently observed in the electrical characterization of real MS contacts. We will first examine how SBH inhomogeneity may alter the shape of I-V plots, then we will discuss the temperature dependence of the ideality factor and the T_0 anomaly, the temperature dependence of the measured SBH, soft reverse characteristics of inhomogeneous MS contacts, and finally, the discrepancy between I-V and C-V measured SBHs.

A. Diodes with a single low-SBH patch

The existence of SBH inhomogeneity may be observed directly in I-V curves. The simulated total current through a circular MS contact, 10 μm in radius, with a uniform SBH of 0.7 V everywhere except for a circular patch, 0.10 μm in radius, which has a SBH of 0.4 V, is shown in Fig. 19. I-V plots obtained at three different temperatures are shown. The dotted line shows the current flow through the low-SBH patch, the solid line shows the current through the uniform region, and the open circles represent the total current through the MS contact. Since current transport across the MS interface is a temperature-activated process, at low temperature the current flow will be dominated by the current flowing through those patches of low SBH, as shown in Fig. 19(a). As was pointed out in the previous

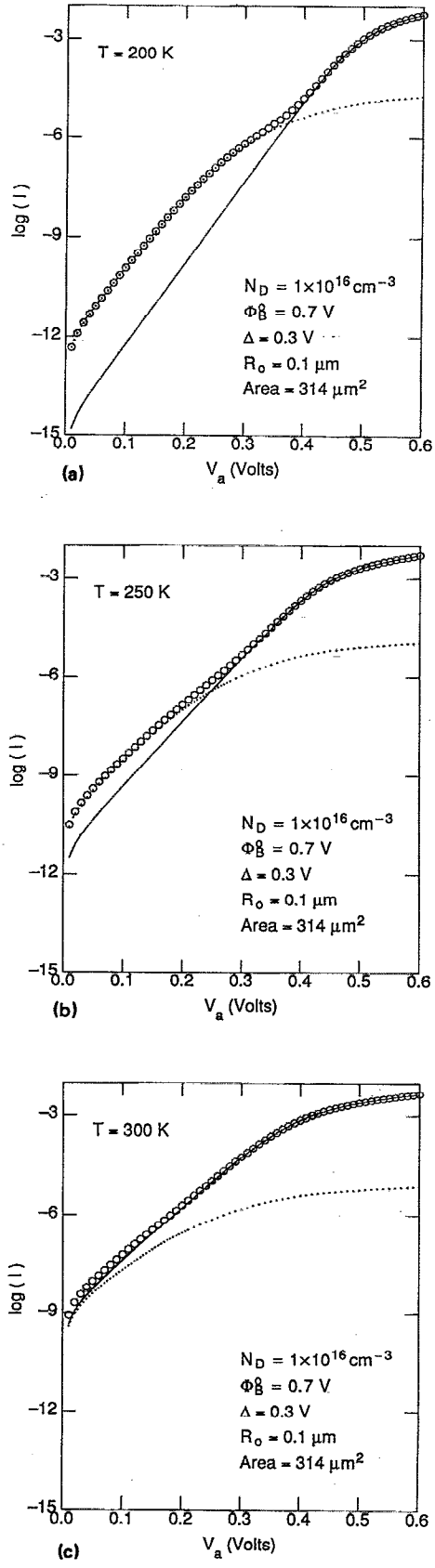

FIG. 19. Numerically determined I-V plots for an inhomogeneous MS contact. The solid line is the numerical result for the current flow through the uniform region, while the dotted line represents the current flow through the low-SBH patch. The circles represent the total current through the inhomogeneous MS contact. (a) Temperature = 200 K. (b) Temperature = 250 K. (c) Temperature = 300 K.

section, the current flow through a low SBH patch is characterized by an ideality factor greater than unity. At high temperature, Fig. 19(c), the current flow is less dominated by the small number of low-SBH regions and the current flow through the uniform region accounts for most of the total current. The ideality factor is close to unity at high temperatures, Fig. 19(c), because the conduction path to the uniform area of the diode is not pinched-off. Since the current density at the low barrier patch is higher than the current density at the "uniform" regions, series resistance becomes important in the low barrier patches at lower values of bias; hence, at some intermediate temperature, the I-V plot shows a double slope structure, as shown in Fig. 19(b), in which there is a linear region at low bias with high ideality factor and another linear region at high bias with an ideality factor close to unity. Since usual SB structures, except those using epitaxial layers, are thicker than that assumed in the numerical simulations (thickness $\geqslant$ twice the semiconductor depletion width), effects due to series resistance may exceed that presently demonstrated.

B. Temperature dependence of the ideality factor

Before we discuss the numerical simulation of the temperature dependence of the ideality factor, much may already be stated simply on the basis of what we have learned from the numerical simulation of individual patches of low SBH. We have shown earlier that pinch-off of low-SBH patches plays a critical role in determining the current transport through individual patches of low SBH and that the ideality factor for the current flow through a single patch of low SBH is given by $n=1+\Gamma$ [see Fig. 16(a) and Eq. (A10)]. With this information, we can already predict the behavior of the ideality factor on temperature for the current flow across some inhomogeneous MS contacts. A schematic summary of some of these dependences of the ideality factor is shown in Fig. 20. Three representative behaviors for the ideality factor are shown in the form of a plot of nk_BT (q times the inverse slope of the I-V plot) versus k_BT. In panel (a), we show three possible forms of SBH inhomogeneity which could produce an ideality factor which remains close to unity over a large temperature range. Panel (a1) shows the trivial situation in which the MS contact is completely uniform, and no spatial variation of the SBH exists; hence, the ideality factor is unity. Panel (a2) reveals the importance of pinch-off of low-SBH regions. When the depletion width is much larger than the "size" of the inhomogeneous regions ($\Gamma\sim 0$), almost complete pinch-off of the low SBH regions occurs, and any lateral potential variation away from the MS interface is quickly damped out; hence, again the ideality factor is close to unity. Panel (a3) shows the situation when there is a very large region of low SBH, relative to the semiconductor depletion width, within the MS contact. Since the low SBH region is very large, almost all of the current flowing across the MS contact flows across this low SBH region. In addition, the very large region of low SBH may not be pinched-off; hence, there is no saddle point, and again the ideality factor remains close to unity.

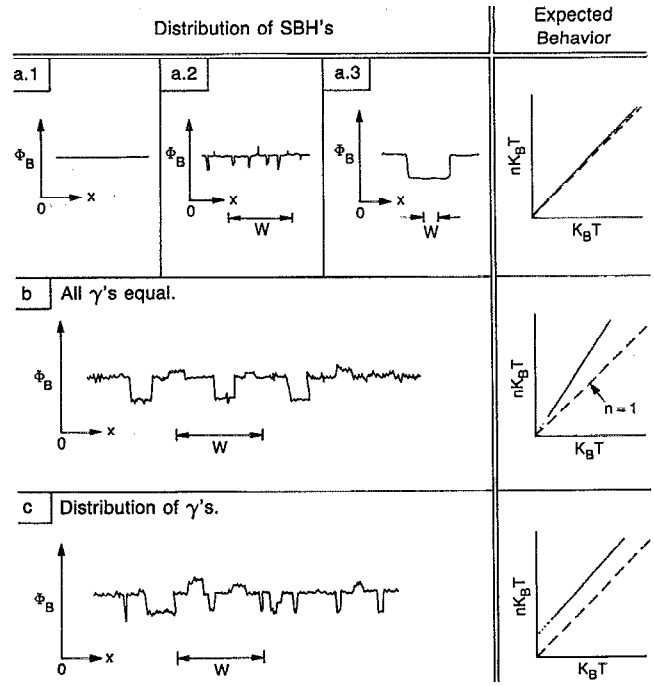

FIG. 20. Schematic illustration of some dependences of the ideality factor of MS contacts with temperature and possible forms of the SBH inhomogeneity which could produce these behaviors.

In order to simulate some of the temperature dependences of the ideality factor shown schematically in Fig. 20, we have first simulated, over a range of temperature, the current flowing through a number of low-SBH patches categorized by different γ's. The total current from these simulations was then summed in well-defined proportions in order to simulate the total current from a large MS contact containing numerous patches of low SBH and large regions of uniform, but higher, SBH. In all of the numerical simulations on the temperature dependence of the ideality factor, we have assumed a substrate of n-type Si with a doping of 1×10^{16} cm^{-3} and that the uniform high SBH region has a SBH of 0.8 V while the low-SBH region has a SBH of 0.4 V. The quantity of the low-SBH patches which were summed to represent the total contact are shown with the figures, along with the total contact area (which includes both the area from the low-SBH patches and the area of the uniform region). In Fig. 21(a), we show a plot of the inverse slope of the I-V plot (nk_BT/q) vs k_BT in which the ideality factor is found to be larger than unity and independent of temperature. This plot was created from numerical simulations of a MS contact in which the total current was dominated by the current flowing through low-SBH patches all characterized by the same γ value, as schematically shown in Fig. 20(b). The ideality factor for the total MS contact is independent of temperature because the ideality factor of the current flowing through each of the identical low-SBH patches is independent of temperature.

In most real MS contacts, there is likely to be a distribution of SBH inhomogeneity (different patch sizes, effec-

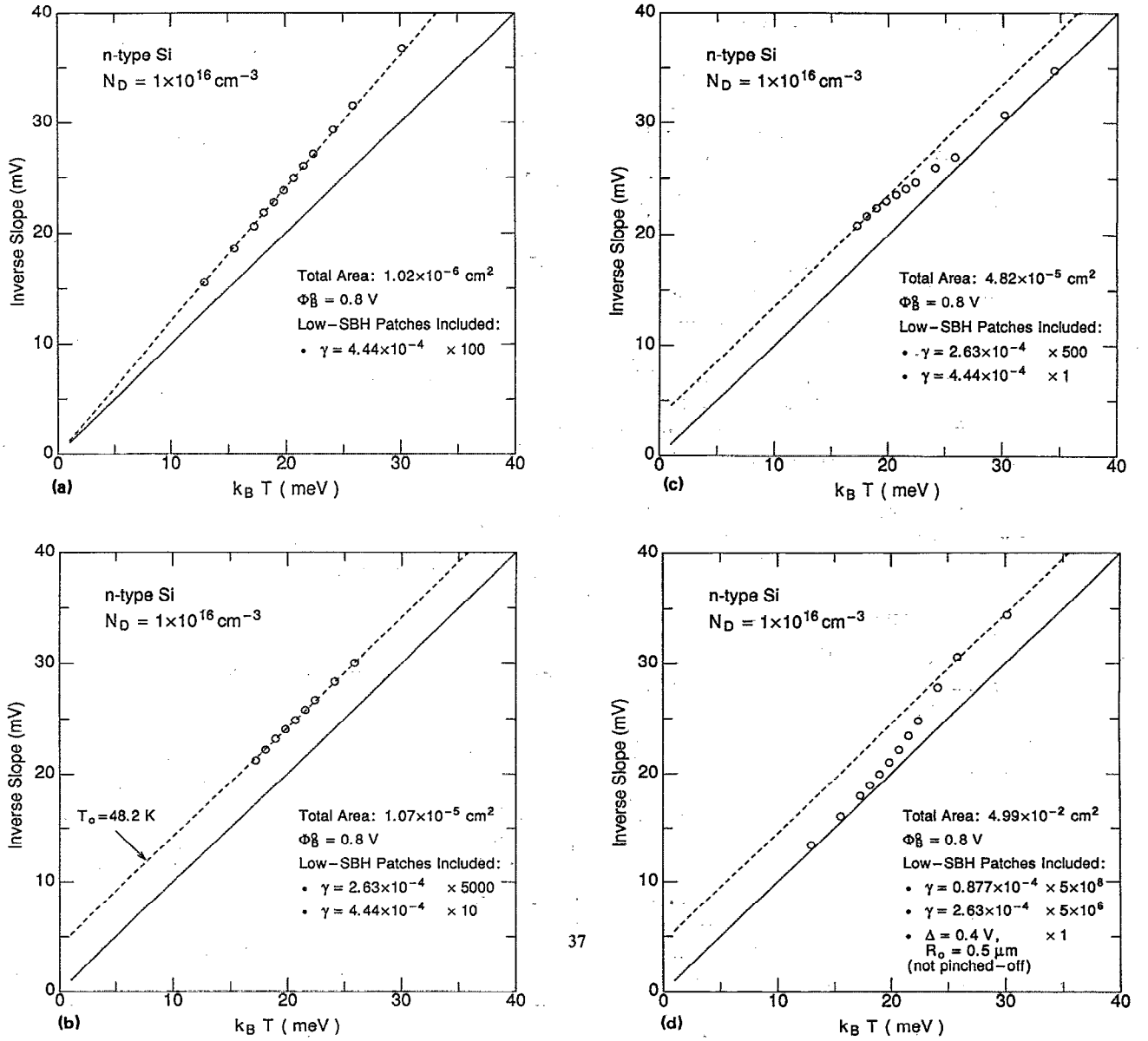

FIG. 21. Plots of the inverse slope of the I-V plot as a function of k_BT for inhomogeneous MS contacts composed of a distribution of low-SBH patches as described in the figures (γ is in units of $V^{1/3}$ $cm^{2/3}$): (a) plot showing a constant ideality factor in excess of unity, (b) plot showing the T_0 anomaly, (c) plot showing $n \approx 1 + T_0/T$ behavior at low temperature and ideal behavior at high temperature, and (d) plot showing ideal behavior at low temperature and $n \approx 1 + T_0/T$ behavior at high temperature.

tive barrier heights, etc.), so that there is a distribution of γ's. Furthermore, the density of patches with a certain γ more likely decreases with γ. Numerical simulations of the temperature dependence of the ideality factor for such a MS contact are shown in Fig. 21(b). The plot reproduces the expected behavior of the ideality factor associated with the T_0 anomaly. Even though patches with only two γ's were used in the simulations, the explanation for the T_0 anomaly is clearly revealed: as the temperature is decreased, current transport becomes dominated by the patches with lower and lower effective barrier height (the patches with larger γ), but the patches with large γ are characterized by a large ideality factor. Therefore, as the temperature is lowered, the measured ideality factor for the MS contact as a whole increases, exhibiting the T_0 anomaly.[18,19] In order to demonstrate the T_0 anomaly over a larger temperature range, numerical simulations involving a larger distribution of γ's would have to be performed. The extrapolated T_0 value from the simulation is 48 K; the approximate value of T_0 from the analytic theory based on a Gaussian distribution of γ's is 59 K [Eq. (A14)]. The agreement with the analytic theory is remarkably good considering that only two γ's were used in the simulations, and the Gaussian distribution is only poorly approximated. It is useful to reiterate that the plot shown in Fig. 21(b) accurately reproduces the classic behavior described by the T_0 anomaly, and it was produced solely on the assumption of a distribution of SBH inhomogeneity, as schematically shown in Fig. 20(c).

Some other forms of the temperature dependence of

the ideality factor (other than those shown in Fig. 20) are observed experimentally and can be demonstrated through numerical simulations. Figure 21(c) shows a plot of the inverse slope of the I-V plot versus k_BT in which the ideality factor has a $1 + T_0/T$ behavior at low temperature and a more ideal behavior, $n \sim 1.00$, at high temperature. This plot, which is similar to some experimental plots shown in the literature,[20] was created by numerical simulations of a MS contact containing patches of two different γ's combined with a large uniform area of higher SBH. At low temperature, the ideality factor is characterized by the current flow through the distribution of low-SBH patches ($n \approx 1 + T_0/T$), while at high temperature, the ideality factor approaches unity (the ideality factor of the large uniform region). The cross-over from the total current dominated by the current through the low-SBH patches to the total current dominated by the current through the uniform region of the diode is similar to that shown in Fig. 19. As the temperature increases, the lower effective SBH of the patches is offset by the much greater area of the uniform region, as a result, most current flows through the uniform region, hence, an ideality factor characteristic of the uniform diode. Figure 21(d) shows an interesting form in which the ideality factor may depend on temperature and which is explainable in terms of SBH inhomogeneity. This MS contact is characterized by an ideality factor which is greater than unity at high temperature and which approaches unity at low temperature. This behavior is caused by SBH inhomogeneity consisting of a few very large patches of low SBH, which are not pinched-off (only one large patch was needed in the simulation), combined with a large number of smaller low-SBH patches. At high temperature, most of the current flows through the large number of smaller low-SBH patches (resulting in an ideality factor greater than unity). At low temperature, however, almost all of the current flows through the very large low-SBH patch, which is large enough that it is not pinched-off, hence an ideality factor close to unity results [see Fig. 20(a3)]. It is difficult to imagine how this particular behavior of the ideality factor, observed experimentally, could be explained by anything but SBH inhomogeneity. All other mechanisms, thus far invoked to explain the ideality factor, predict behaviors contrary to this particular experimental observation.[21]

C. Temperature dependence of the effective barrier height

In many experimental studies in which I-V plots are measured as a function of temperature, it is frequently observed that the measured I-V SBH is a function of temperature. This weak temperature dependence is usually explained in terms of the weak temperature dependence of the semiconductor band gap; however, it is sometimes found that the temperature coefficient of the SBH differs substantially from the band-gap temperature coefficient and is often of the opposite sign. The existence of SBH inhomogeneity offers a possible explanation for this anomalous temperature dependence. Numerical simulations, as a function of temperature, for a MS contact, containing a single low-SBH patch 0.026 μm in radius and with a SBH of 0.4 V, were made, and the effective SBH, Φ_{EFF}, was determined from the zero bias intercept of the numerical I-V plot (see Fig. 22). In the numerical simulations, the band gap was intentionally held fixed, independent of temperature, so the temperature dependence of the effective barrier height only contains contributions from the presence of inhomogeneity. Figure 22 clearly reveals a temperature-dependent effective SBH due solely to the existence of inhomogeneity.

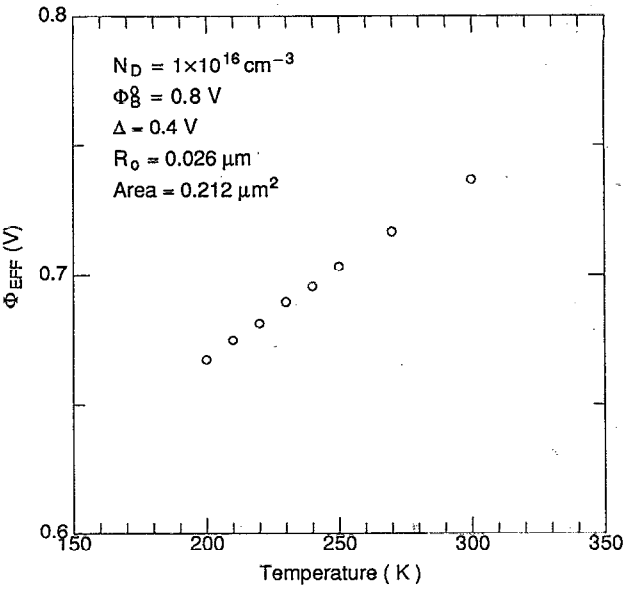

FIG. 22. Variation of the effective barrier height with temperature of a MS contact containing a low-SBH patch.

D. Reverse characteristics

An anomalous characteristic associated with the electrical characterization of real MS contacts at reverse bias is the form of the reverse current as a function of bias. It is observed that the reverse current does not saturate with reverse bias, rather it increases with voltage up to the point of break-down.[10] This soft reverse characteristic is often explained in terms of a bias-dependent barrier height, and the weak bias-dependence of the SBH due to image force lowering is often cited as the possible source. If image force lowering is the only source of bias-dependence of the SBH, then the logarithm of the reverse current should be proportional to the 1/4 power of the band-bending, V_{bb}. This dependence is frequently observed experimentally; however, in many cases the observed voltage dependence of the barrier height determined from the reverse characteristics exceeds the expected result based on image force lowering.[10,22] The existence of SBH inhomogeneity offers a natural explanation for the soft reverse characteristics observed experimentally. Depending on the nature of the inhomogeneity, the logarithm of the reverse current at large bias may vary with V_{bb}^{α} where α could be 1/3 or larger according to the analytic theory [see Eq. (A9) and Ref. 14]. Note that, aside from a $V_{bb}^{1/4}$ dependence based on

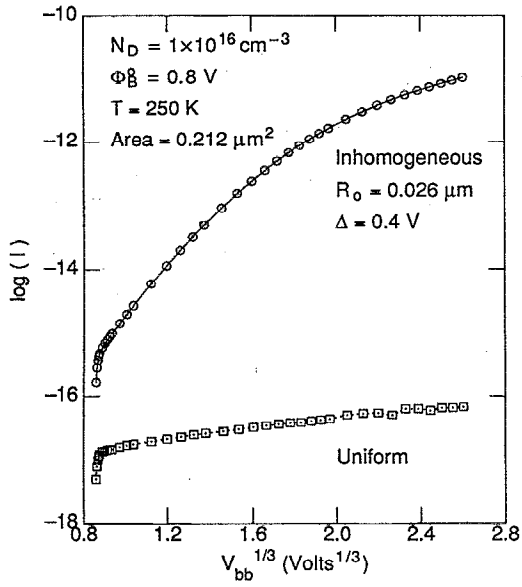

FIG. 23. Variation of the logarithm of the reverse current as a function of V_{bb}. The circles are the numerical simulation of an inhomogeneous MS contact and the squares are the numerical simulation of a uniform MS contact. The lines are guides for the eyes.

image force lowering, there is no straightforward explanation for the soft reverse characteristics observed experimentally if a spatially uniform Schottky barrier is assumed. In Fig. 23 we show numerical simulations of the logarithm of the reverse current as a function of $V_{bb}^{1/3}$ for a uniform MS contact (shown as the squares) and a contact containing a single circular patch of low SBH amidst a region of higher SBH (shown as circles). No image force lowering was allowed in the simulation. Note that, as expected, the reverse current for the uniform MS contact exhibits a behavior close to saturation (the deviation coming from generation current), while the reverse current for the inhomogeneous contact is strongly dependent on reverse bias. There are linear regions in the plot which seem well-described by a $V_{bb}^{1/3}$ dependence, but a plot as a function of $V_{bb}^{1/4}$ also shows a large linear region, which indicates the difficulty in determining the exact dependence of the reverse current on bias. Regardless of the exact dependence of the reverse current on V_{bb} for the inhomogeneous MS contact, the most significant point shown by the plots in Fig. 23 is that the reverse characteristics in the presence of SBH inhomogeneity may be much more dependent on V_{bb} than would be observed for a uniform diode. The origin of this effect will be discussed later. These simulations suggest that the various assumptions developed to explain the strong dependence, for some MS contacts, of the reverse current on V_{bb}, such as the model proposed by Andrews and Lepselter which is based on interface states,[10] may not be necessary when there is the existence of SBH inhomogeneity.

E. Discrepancy between *C-V* and *I-V* determined barrier heights

It is frequently observed experimentally that the SBH determined from measurements of capacitance of the MS contact as a function of voltage exceeds the *I-V* measured SBH.[23] Although this discrepancy could be explained by the existence of excess capacitance at MS contacts due to an interfacial dielectric layer or to trap states in the semiconductor, the existence of SBH inhomogeneity offers another explanation. In order to show this discrepancy directly we have performed numerical simulations of the junction capacitances. The capacitance and conductance were calculated for the MS contact based on ac small signal analysis[24] at a driving frequency of 100 kHz and at reverse bias voltages up to 2.6 V. For uniform MS contacts, it was found that the intercept of the voltage axis in a plot of C^{-2} versus voltage gave the barrier height of the MS contact less V_n, in good agreement with the SBH obtained by *I-V*. In Fig. 24(a) we show the *C-V* plot of an inhomogeneous diode in which 16% of the total contact area consisted of a circular region of SBH equal to 0.4 V, with the remaining region characterized by a SBH of 0.8 V. The points from the numerical simulations are shown as the circles and the solid line represents a linear least-squares fit. The SBH determined from the simulation is 0.72 V. This is close to the arithmetic mean, weighted by the area fraction, for the two SBH regions, 0.736 V. Other simulations (not shown) have indicated that the SBH measured by *C-V* is always close to the weighted arithmetic average of the SBHs in the inhomogeneous MS contact. This result seems to be independent of the geometry of the inhomogeneity, temperature, and doping (including doping inhomogeneity). Numerical simulations of the *I-V* characteristics for the inhomogeneous MS contact is shown in Fig. 24(b); the circles represent the simulated points while the dashed line is a linear least-squares fit to the linear region of the *I-V* plot. The SBH determined from the zero bias intercept and assuming thermionic emission as the current transport mechanism is determined to be 0.62 V. This is well below the *C-V* measured SBH and the weighted arithmetic average of the SBHs. The reason for the discrepancy between the *I-V* and *C-V* measured SBH is clear. The current in the *I-V* measurement is dominated by the current which flows through the region of low SBH. Since the low-SBH patch is pinched-off, the effective SBH of the patch is the potential at the saddle point, which has a potential with respect to the metal FL of about 0.52 V for this particular contact. Hence the measured *I-V* barrier height is significantly lower than the weighted arithmetic average of the SBHs. The *C-V* measured barrier height, on the other hand, is influenced by the distribution of charge at the depletion region boundary. As evidenced by the numerical simulations, this charge distribution follows the weighted arithmetic average of the SBH inhomogeneity; hence, the *C-V* determined barrier height is close to the weighted arithmetic average of the SBHs. It should be noted that since the low-SBH patches are more effectively pinched-off when the semiconductor doping is low, discrepancies between *I-V* and *C-V* measurements should be less at lower doping levels. This trend is, indeed, observed experimentally.[23]

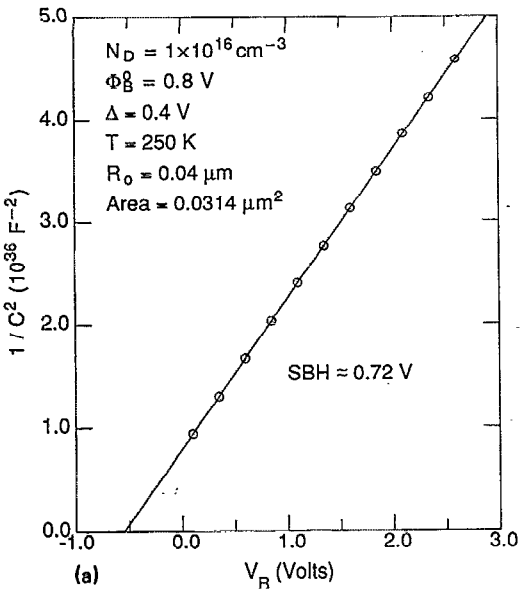

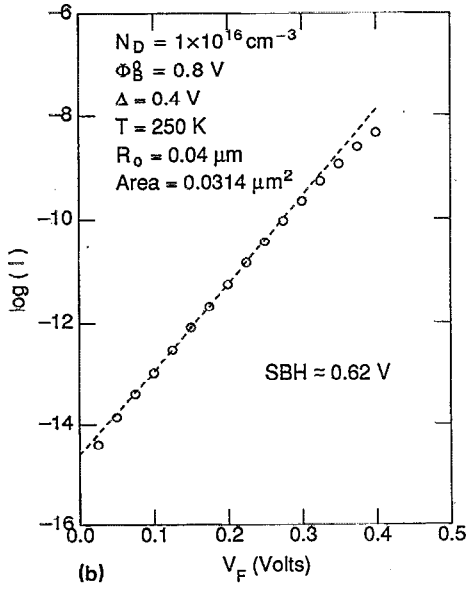

FIG. 24. (a) Numerically determined *C-V* plot, indicating a SBH of about 0.72 V. (b) Numerically determined *I-V* plot for the same MS contact as shown in (a) and indicating a SBH of about 0.62 V.

VI. DISCUSSION

The discussion of the electrical characteristics of MS contacts with SBH inhomogeneity would be superfluous were it not for the fact that there is increasing experimental evidence for the possible existence of spatial inhomogeneity in the SBH at MS interfaces. The assumption of a unique FL pinning position at the MS interface may not hold true in many, if not most, experimental MS contacts. Differences in the crystal symmetry of the metal with respect to the semiconductor,[11] differences in interfacial reconstruction,[12] and differences in the orientation of the semiconductor have all been shown to produce differences in the measured SBH of MS contacts. As has been recently demonstrated, a variation in the orientation at a MS interface, due to localized faceting of the interface, for example, may directly exhibit the features of SBH inhomogeneity. This is, indeed, the situation for $NiSi_2$ on Si (100), and since a variation in the processing allows control of the extent of faceting of the interface, the SBH inhomogeneity may be directly controlled.[25] There are certainly other sources for SBH inhomogeneity which may be imagined. For example, there may be a mixture of different metallic phases with different SBHs at a MS interface due to incomplete interfacial reaction. Additionally, there may be doping inhomogeneity at the MS interface, dopant clustering, for example. Contamination at the MS interface, whether particulates or undesirable reaction products (oxides and carbides, for example), are often present at the MS interfaces of diodes prepared by the routine processing methods used in the semiconductor electronics industries. These contaminants may act directly to introduce inhomogeneity or they may simply promote inhomogeneity, through the generation of defects, additional interfacial chemical phases, etc. Even in the absence of a chemical contaminant, SBH inhomogeneity may be present. Interface nonplanarity, due to reaction spiking for example, may contribute to or accentuate SBH inhomogeneity (see Fig. 13), thus effectively increasing or decreasing the apparent γ of low-SBH patches. Finally, there are numerous structural defects, grain boundaries, dislocations, stacking faults, at MS interfaces, and these may contribute to SBH inhomogeneity.

The numerical simulations which we have presented are not the first simulations of SBH inhomogeneity. Some of the first numerical investigations of the potential distribution associated with SBH inhomogeneity were performed by Freeouf *et al.*[26,27] In their simulations, they noted the effect of potential pinch-off on regions of low SBH with dimensions comparable to the Debye length of the semiconductor. Their simulations were also based on a device analysis program which simultaneously solved the Poisson equation and the electron and hole continuity equations. Although they only employed a strip geometry for their inhomogeneous MS contact, their results are quite similar to the potential distributions we have discussed earlier. Ohdomari and Aochi have also examined the potential contours associated with SBH inhomogeneity at the MS interface by using an approximation to the two-dimensional Poisson equation.[28] Their work, however, did not show the existence of potential pinch-off of the low-SBH patch because their boundary condition for the MS interface was not fixed by the interface SBH. Instead, the interface potential was determined (unphysically) from the potentials within the semiconductor. More recently, Bastys *et al.* modeled the potential distribution and electron transport for isolated diodes with a surrounding annulus of different SBH. Although these calculations were aimed at simulating observed macroscopic inhomogeneities,[29] the effect of pinch-off was clearly demonstrated. These authors also correctly noted the significant effect this has on determining an effective SBH from current-voltage measurements. From these isolated simulations previously performed, it is clear that pinch-off is an important and general feature of inhomogeneous MS contacts, at least

when the dimensions of the low-SBH regions are on the order of the dimensions of the semiconductor depletion width. The present work is the first systematic and quantitative study of the pinch-off effect. In particular, the bias-dependence of the saddle point potential, little discussed in previous works, is the key to understanding electron transport at inhomogeneous MS contacts in general. Other factors and parameters which influence the potential distribution have been identified and their effects discussed. From these discussions and the comparison with a recent analytic theory, accurate predictions of the potential for arbitrary SBH distributions are possible for the first time.

Experimentally, one of the most common means of characterizing the electrical properties of SB diodes is by measuring the current across the diode as a function of bias (an I-V measurement). In addition to the SBH, one parameter obtained from a measurement of this sort is the ideality factor. From the earliest I-V measurements performed on SB diodes, it was noted that the ideality factor for many diodes deviated significantly from unity.[5] Explanations for this deviation of the ideality factor from unity ranged from assumptions of generation recombination current in the space-charge region[9] to interface dielectric layers or field emission or thermionic field emission.[30] Only recently has it been shown that an ideality factor in excess of unity is consistent with the existence of SBH inhomogeneity.[14] We have confirmed the theoretically predicted dependence of the ideality on SBH inhomogeneity through numerical simulations. This correlation with SBH inhomogeneity is especially significant for not only does it offer a reasonable explanation for the general observation of ideality factors in excess of unity, but it also provides a natural explanation for the observed variation of the ideality factor with processing of the MS contact.[31] Different processing could easily influence the form of the inhomogeneity at the MS interface, resulting in different γ's and, hence, different observed ideality factors. SBH inhomogeneity also offers an explanation for the diversity of behaviors observed on the temperature dependence of the ideality factor, e.g., Fig. 21.[19,32–35] In particular, the mysterious T_0 anomaly was shown to be related to SBH inhomogeneity. Traditional explanations for this T_0 anomaly include a distribution of interface states or an interfacial inversion layer.[7,8] However, in most experimental studies, there is little or no evidence for this distribution in interface states or an interfacial inversion layer. The existence of SBH inhomogeneity does seem to offer a very reasonable explanation for this anomaly.

The existence of SBH inhomogeneity may also alter the overall appearance of the measured I-V curves. For example, the types of plots shown in Fig. 19 are frequently observed experimentally,[32–34] and the excess current at low bias is commonly attributed to edge leakage current associated with carrier recombination in the high field region at the diode edges.[9] While edge leakage current may be a factor in experimentally prepared diodes, especially those without guard rings, it is unclear why edge-related currents have invariably been attributed to generation-recombination in the depletion region. As shown in Fig. 19, the presence of a patch of low SBH in an otherwise uniform diode is sufficient to reproduce the excess current observed at low bias. Experimentally, however, it is sometimes observed that the current measured from a SB diode is proportional to the perimeter of the diode rather than the diode area. This observation would certainly indicate that edge leakage current is the dominant component of the total current flowing through the SB diode. It is not necessary, however, to attribute this current to carrier recombination at the diode edges. SBH inhomogeneity offers a natural explanation for the observed edge leakage current without having to introduce any additional current transport mechanisms. If a MS contact contains a distribution of low-SBH patches, it is likely that some of these low-SBH patches will be found near the diode edges. Because low-SBH patches near the diode edges are not completely surrounded by high barrier regions, they are less pinched-off relative to patches away from the diode edges (see Fig. 12). Patches which are less pinched-off have a lower effective SBH, and, hence, the current flow through these patches is greater. For certain γ's, doping levels, and temperatures, the current through these low-SBH patches at the diode edges may be much greater than the current which flows through the rest of the diode, thereby resulting in a total current proportional to the diode perimeter. For the diode structures shown in Fig. 12, the extrapolated saturation current increases from $\sim 5.5\times 10^{-15}$ A/μm for the diode geometry of Fig. 12(a) to $\sim 3.2\times 10^{-11}$ A/μm for the diode geometry of Fig. 12(c). This represents an almost ten thousand-fold increase in current, even though the total diode area and low and high SBH areas remained the same. This suggests that some of the experimentally observed edge leakage current may be a natural result of SBH inhomogeneity.

The soft reverse characteristics of real MS contacts may also be readily understood in terms of SBH inhomogeneity. For inhomogeneous MS contacts, the reverse current may be dominated by the current which flows through the low-SBH patches, which is controlled by the potential at the saddle point. Increasing reverse bias drops the potential at the saddle point, hence the reverse current increases with increasing reverse bias and does not saturate. Different forms of inhomogeneity will have different dependences of the saddle point potential on reverse bias, so the dependence of the reverse current on V_{bb} will be different [Eq. (A9)]. It is also important to note that at sufficiently high reverse bias the low-SBH patches may no longer be pinched-off. As a result, it may be expected, at least in theory, that the $V_{bb}^{1/3}$, etc. dependence of the reverse current on bias may begin to saturate at high values of bias before generation and ionization current begin to dominate, although this effect has rarely been observed experimentally. In addition to the bias dependence of the reverse current, the analytic theory also predicts that this reverse current at large bias will be strongly temperature-dependent when there exists a distribution of SBH inhomogeneity. Although we have not performed numerical simulations of the temperature dependence of the reverse characteristics of a MS contact containing a distribution of

SBH inhomogeneity, this strong temperature dependence may be expected to exist because the temperature dependence is based on the same phenomenon which gives rise to the T_0 anomaly, which we have demonstrated numerically [see Fig. 21(b)].

Throughout the numerical simulations, we have attempted to highlight some of the diverse electrical behavior which can occur with the existence of SBH inhomogeneity. Numerical simulations show that nonlinearities in the *I-V* plot, the discrepancy between SBHs determined by *I-V* and *C-V*, the T_0 anomaly, the temperature dependence of the barrier height, the soft reverse characteristics and other behavior may occur as a result of SBH inhomogeneity. These numerical simulations offer an explanation to the diverse range of behavior observed experimentally for a large range of MS contacts for many different MS. Although other mechanisms may be active, in many cases there is no need to introduce additional *ad hoc* theories to the existing theory of thermionic emission in the presence of SBH inhomogeneity.

VII. CONCLUSIONS

We have shown through numerical simulations of spatially nonuniform MS contacts that the existence of SBH inhomogeneity may explain a host of anomalous behavior frequently observed in the electrical characterization of MS contacts. In particular, the ideality factor, nonlinearity in *I-V* plots, the edge leakage current, the discrepancy between *C-V* and *I-V* measured barrier heights, the T_0 anomaly, and the soft reverse current may all be explained in terms of SBH inhomogeneity. Numerical simulations reveal that these abnormal behaviors are possibly controlled by the important phenomenon of potential pinch-off at inhomogeneous SB diodes. It is also important to note that all of these results were derived on the basis of SBH inhomogeneity alone, i.e., there was no need to postulate the existence of interfacial layers, interface state distributions, etc.

With the realization that there may be significant variation in the interfacial SBH in real MS contacts, we are now better able to examine the physics behind the formation of the SB. A spatially varying SBH at a MS interface is not consistent with the concept of FL pinning. Instead, a formation mechanism of the SB which is strongly dependent on the local structure of the MS interface is suggested. To better elucidate the link between the structural and electronic properties of the MS interface, controlled studies of well-characterized MS interfaces are needed. Epitaxial MS interfaces provide a valuable starting point for studies of SBH mechanisms. Experimental studies along these lines, should turn out to be most fruitful.

APPENDIX A: SUMMARY OF THE ANALYTIC THEORY

The analytic theory of SBH inhomogeneity is based on the use of a dipole layer approximation to accurately predict the potential distribution associated with spatial variation of the SBH at the MS interface.[14] For the geometry of circular patches of low SBH used in most of the numerical simulations, the expected potential distribution along a line normal to the MS interface and passing through the center of the low-SBH circular patch is given by

$$V(z)=V_{bb}(1-z/W)^2-\Delta\left(1-\frac{z}{(z^2+R_0^2)^{1/2}}\right)+V_n+V_a, \tag{A1}$$

where V_{bb} is the total band bending ($V_{bb}=\Phi_B^0-V_a-V_n$, Φ_B^0 is the average SBH, and V_n is the potential separation between the CBM and FL in the semiconductor far from the MS interface), W is the depletion width [given by $W\approx(2V_{bb}\eta)^{1/2}$, where $\eta\equiv\epsilon_s/qN_D$, and ϵ_s is the permittivity of the semiconductor], Δ is the local SBH deviation from the average SBH, and R_0 is the low-SBH patch radius as discussed earlier. This expression was used to create the solid line shown in Figs. 5 through 10. In the absence of any adjustable parameters, the analytic expression provides an essentially perfect description of the potential contours associated with SBH inhomogeneity, even though the analytic theory does not account for the actual carrier densities in the depletion region and it assumes the validity of a single, constant depletion width. For the geometry of low-SBH strips of width, L_0, and of infinite length surrounded by a region of higher SBH the potential normal to the MS interface and passing through the middle of the strip is given as

$$V(z)=V_{bb}(1-z/W)^2-\frac{\Delta}{\pi}\tan^{-1}\frac{|x|+L_0/2}{z}+\frac{\Delta}{\pi}\tan^{-1}\frac{|x|-L_0/2}{z}+V_n+V_a. \tag{A2}$$

These equations may be readily used to determine criteria for potential pinch-off of the low-SBH regions. For the circular patch geometry, the criterion for pinch-off is

$$\frac{\Delta}{V_{bb}}>\frac{2R_0}{W}, \tag{A3}$$

and for the strip geometry, the criterion for pinch-off is

$$\frac{\Delta}{V_{bb}}>\frac{\pi L_0}{2W}. \tag{A4}$$

For purposes of analytically determining the transport of current across the MS interface, the dipole layer in the analytic theory was further approximated as a point dipole. The potential distribution predicted from this approximation for the circular geometry is given by

$$V(z)=V_{bb}(1-z/W)^2-\frac{\Delta R_0^2}{2z^2}+V_n+V_a, \tag{A5}$$

and this is shown as the dashed line in Fig. 6. Of course the agreement between this analytic expression and the numerical simulations is poor near the MS interface. Near the saddle point, however, the agreement is reasonable, and beyond this region, the agreement is very good. It follows from Eq. (A5) that the potential at the saddle point is approximately given by

$$V(z)_{\text{saddle}} \approx V_{\text{bb}}\left[1-3\left(\frac{R_0^2}{4\eta V_{\text{bb}}^2}\right)^{1/3}\right]+V_n+V_a$$

$$=\Phi_B^0-\gamma(V_{\text{bb}}/\eta)^{1/3}=\Phi_B^0-3V_{\text{bb}}\Gamma, \tag{A6}$$

where

$$\gamma \equiv 3(\Delta R_0^2/4)^{1/3} \tag{A7}$$

and

$$\Gamma \equiv \left(\frac{\Delta R_0^2}{4\eta V_{\text{bb}}^2}\right)^{1/3}=\left(\frac{1}{27\eta V_{\text{bb}}^2}\right)^{1/3}\gamma. \tag{A8}$$

Using the point dipole approximation, equations for the expected current flow through regions of low SBH are derivable from the analytic theory. For the geometry of circular patches of low SBH amidst a region of higher SBH, the current, ideality factor, and effective SBH of the low-SBH patch are predicted to be

$$I_{\text{patch}} \approx A^* A_{\text{eff}} T^2 \exp\left(-\beta\Phi_B^0+\frac{\beta\gamma V_{\text{bb}}^{1/3}}{\eta^{1/3}}\right)$$

$$\times[\exp(\beta V_a)-1], \tag{A9}$$

$$n=1+\frac{\gamma}{3\eta^{1/3}V_{\text{bb}}^{2/3}}=1+\Gamma, \tag{A10}$$

$$\Phi_{\text{eff}}=\Phi_B^0-\frac{\gamma V_{\text{bb}}^{1/3}}{\eta^{1/3}}, \tag{A11}$$

where A^* is the effective Richardson's constant and A_{eff} is the effective area of the low-SBH patch given by

$$A_{\text{eff}}=\frac{4\pi\gamma\eta^{2/3}}{9\beta V_{\text{bb}}^{2/3}}. \tag{A12}$$

For measurements at constant applied bias and assuming a Gaussian distribution of low-SBH circular patches characterized by a distribution of γ's with standard deviation, σ, the temperature dependence of the ideality factor is predicted to be

$$n=1+\beta\xi\kappa V_{\text{bb}}^{\xi-1}=1+T_0/T, \tag{A13}$$

where

$$T_0=\xi\kappa V_{\text{bb}}^{\xi-1}q/k_B \tag{A14}$$

and $\kappa=\sigma^2/2\eta^{2/3}$ and $\xi=2/3$. This is the temperature dependence of the ideality factor observed in the classic T_0 anomaly.

[1] J. Bardeen, Phys. Rev. **71**, 717 (1947).
[2] V. Heine, Phys. Rev. A **138**, 1689 (1965).
[3] J. Tersoff, Phys. Rev. Lett. **52**, 465 (1984).
[4] W. E. Spicer, I. Lindau, P. R. Skeath, C. Y. Su, and P. W. Chye, Phys. Rev. Lett. **44**, 420 (1980).
[5] S. M. Sze, *Physics of Semiconductor Devices* (Wiley, New York, 1981).
[6] E. H. Rhoderick and R. H. Williams, *Metal Semiconductor Contacts* (Clarendon, Oxford, 1988).
[7] J. D. Levine, J. Appl. Phys. **42**, 3991 (1971); Solid-State Electron. **17**, 1083 (1974).
[8] C. R. Crowell, Solid-State Electron. **20**, 171 (1977).
[9] A. Y. C. Yu and E. H. Snow, J. Appl. Phys. **39**, 3008 (1968).
[10] J. M. Andrews and M. P. Lepselter, Solid State Electron. **13**, 1011 (1970).
[11] R. T. Tung, Phys. Rev. Lett. **52**, 461 (1984).
[12] D. R. Heslinga, H. H. Weitering, D. P. van der Werf, T. M. Klapwijk, and T. Hibma, Phys. Rev. Lett. **64**, 1589 (1990).
[13] C. J. Palmstrom, T. L. Cheeks, H. L. Gilchrist, J. G. Zhu, C. B. Carter, and R. E. Nahory, Mater. Res. Soc. **EA-21**, 63 (1990).
[14] R. T. Tung, Appl. Phys. Lett. **58**, 2821 (1991), Phys. Rev. B (to be published).
[15] M. R. Pinto, in 1991 ULSI Science and Technology, Electrochem. Soc. Proc. (to be published, 1991).
[16] M. R. Pinto, W. M. Coughran, Jr., C. S. Rafferty, R. K. Smith, and E. Sangiorgi, in *Computational Electronics*, edited by K. Hess, J. P. Leburton, and U. Ravaioli (Kluwer, Boston, 1990).
[17] I. Ohdomari and K. N. Tu, J. Appl. Phys. **51**, 3735 (1980).
[18] F. A. Padovani and G. G. Sumner, J. Appl. Phys. **36**, 3744 (1965).
[19] A. N. Saxena, Surf. Sci. **13**, 151 (1969).
[20] See, for example, Fig. 4 in M. O. Aboelfotoh, J. Appl. Phys. **66**, 262 (1989).
[21] See, for example, Fig. 9 in M. O. Aboelfotoh and K. N. Tu, Phys. Rev. B **34**, 2311 (1986).
[22] G. H. Parker, T. C. McGill, and C. A. Mead, Solid-State Electron. **11**, 201 (1968).
[23] See, for example, A. Thanailakis, J. Phys. C **8**, 655 (1975); A. Thanailakis and A. Rasul, J. Phys. C **9**, 337 (1976); Zuzanna Liliental-Weber, R. Gronsky, J. Washburn, N. Newman, W. E. Spicer, and E. R. Weber, J. Vac. Sci. Technol. B **4**, 912 (1986).
[24] S. E. Laux, IEEE Trans. Electron Dev. **ED-32**, 2028 (1985).
[25] R. T. Tung, A. F. J. Levi, J. P. Sullivan, and F. Schrey, Phys. Rev. Lett. **66**, 72 (1991).
[26] J. L. Freeouf, T. N. Jackson, S. E. Laux, and J. M. Woodall, Appl. Phys. Lett. **40**, 634 (1982).
[27] J. L. Freeouf, T. N. Jackson, S. E. Laux and J. M. Woodall, J. Vac. Sci. Technol. **21**, 570 (1982).
[28] I. Ohdomari and H. Aochi, Phys. Rev. B **35**, 682 (1987).
[29] A. I. Bastys, V. B. Bikbaev, J. J. Vaitkus, and S. C. Karpinskas, Litovskii Fizicheskii Sbornik **28**, 191 (1988).
[30] F. A. Padovani and R. Stratton, Solid-State Electron. **9**, 695 (1966); V. L. Rideout and C. R. Crowell, Solid-State Electron. **13**, 993 (1970); H. C. Card and E. H. Rhoderick, J. Phys. D. **4**, 1589 (1971).
[31] See, for example, M. O. Aboelfotoh, J. Appl. Phys. **66**, 262 (1989).
[32] M. O. Aboelfotoh, J. Appl. Phys. **64**, 4046 (1988).
[33] M. O. Aboelfotoh, A. Cros, B. G. Svennson, and K. N. Tu, Phys. Rev. B **41**, 9819 (1990).
[34] A. Zussman, J. Appl. Phys. **59**, 3894 (1986).
[35] B. Tuck, G. Eftekhari, and D. M. de Cogan, J. Phys. D **15**, 457 (1982).